

Determination of Viscoelastic Material Properties and Impact Force from Measurements on Impacted Bodies

by

Sven Ödeen

Determination of Viscoelastic Material
Properties and Impact Force from
Measurements on Impacted Bodies

by

Sven Ödeen

Akademisk avhandling

som med vederbörligt tillstånd av Tekniska Fakultetsnämnden vid
Högskolan i Luleå för avläggande av teknisk doktorsexamen kommer att
offentligt försvaras i Högskolans sal α117 (LKAB-salen), fredagen den 17
september 1993, kl. 09.00.

PREFACE

This work has been carried out at the Division of Solid Mechanics, Luleå University of Technology, and, during my one-year stay in Marseille, at Laboratoire de Mécanique et d'Acoustique, CNRS.

I would like to express my gratitude to my supervisor Professor Bengt Lundberg. His guidance and friendship have been of outstanding importance for the completion of this thesis.

I thank Doctor Robert Blanc for his support and generous hospitality during my stay in Marseille.

I am greatly indebted to Doctor Irina Trendafilova for our intensive and stimulating cooperation during her visit in Luleå.

I am also grateful to Mr. Mats Nilsson. His support and good humour have been valuable during the sometimes long hours in the laboratory.

Finally, I am indebted to the Carl Trygger Research Foundation and the Research Council of Norrbotten for financial support of this work, and to the Swedish Institute for supporting my stay in Marseille.

Luleå in August 1993

Sven Ödeen

ABSTRACT

Methods are presented for identification of linear and nonlinear viscoelastic materials and for prediction of impact force on the basis of measurements made on impacted bodies. The complex modulus is identified from measured end-point accelerations of an impacted rod specimen, and *in-situ* from measured strains at three sections of a rod-like member of an impacted structure. The two methods for identification of complex modulus have been tested experimentally on two polymers, viz., polypropylene and polyamide 6, and results have been obtained in frequency ranges of up to two decades. Furthermore, the complex modulus of polyoximethylene has been determined during creep recovery by using the method based on acceleration measurements. Moreover, a method is proposed for identification of nonlinear viscoelastic materials on the basis of displacements measured at two sections of an impacted rod specimen. The displacements were measured by means of electro-optical displacement transducers. The first step of the method is model identification, i. e., choice of constitutive model. The second is parameter identification, i. e., determination of the parameters of the model chosen. The method has been applied to five polymers of interest in engineering, viz., polypropylene, polyamide 6, polyoximethylene, high density polyethylene, and 60 percent carbon-black filled natural rubber. Finally, a method is established which permits prediction of impact force history from the velocity response of each impacting body to an impulsive force applied to its impact face, and the impact velocity. It is assumed that the impacting bodies behave linearly. The method has been applied to several cases of impact between linearly elastic and linearly viscoelastic bodies. The predicted impact forces are compared to impact forces measured in impact tests. Generally, there is a good agreement.

THESIS

This thesis comprises a survey and the following five papers:

- A. S. Ödeen and B. Lundberg, Determination of complex modulus from measured end-point accelerations of an impacted rod specimen. To appear in *Journal of Sound and Vibration* **163** (1993).
- B. B. Lundberg and S. Ödeen, In-situ determination of complex modulus from strain measurements on an impacted structure. To appear in *Journal of Sound and Vibration* (1993).
- C. S. Ödeen and R. H. Blanc, Effects of load and recovery time on the complex modulus of polyoximethylene. Submitted for publication (1993).
- D. I. N. Trendafilova, S. Ödeen and B. Lundberg, Identification of viscoelastic materials from two-point electro-optical displacement measurements on an impacted rod. Submitted for publication (1993).
- E. S. Ödeen and B. Lundberg, Prediction of impact force by impulse response method. *International Journal of Impact Engineering* **11**, 149-158 (1991).

CONTENTS

1. INTRODUCTION	1
2. EXTENSIONAL WAVES IN VISCOELASTIC RODS	3
3. IDENTIFICATION OF LINEAR VISCOELASTIC MATERIALS	5
3.1 Theory	5
3.2 Experiments and results	7
3.3 Complex modulus during creep recovery	9
3.4 Concluding remarks	10
4. IDENTIFICATION OF NONLINEAR VISCOELASTIC MATERIALS	13
4.1 Theory	13
4.2 Experiments and results	15
4.3 Concluding remarks	15
5. PREDICTION OF IMPACT FORCE	17
5.1 Theory	17
5.2 Experiments and results	19
5.3 Concluding remarks	20
6. CONCLUSIONS	21
REFERENCES	23

APPENDED PAPERS

A. Determination of complex modulus from measured end-point accelerations of an impacted rod specimen.	A1-A14
B. In-situ determination of complex modulus from strain measurements on an impacted structure.	B1-B10
C. Effects of load and recovery time on the complex modulus of polyoximethylene.	C1-C9
D. Identification of viscoelastic materials from two-point electro-optical displacement measurements on an impacted rod.	D1-D15
E. Prediction of impact force by impulse response method.	E1-E19

INTRODUCTION

The theory of viscoelasticity stems from the early work by, e. g., Maxwell, Kelvin and Boltzmann. The development of this theory and of methods for characterizing and analysing viscoelastic materials have been motivated by the development and application of polymeric materials.

Polymers, as well as some metals, behave viscoelastically when they are subjected to dynamic loads. Therefore, knowledge of their dynamic properties is essential. An important dynamic problem is that of impact. The responses of impacted bodies can be used to determine dynamic properties of the bodies and of their materials. In this thesis measured responses are used to identify viscoelastic materials and to predict impact force.

Identification of a material from the mechanical response of an excited body is an example of an *inverse problem* which can be formulated as follows: Given the excitation, the response and the geometry of the body; determine the mechanical properties of the material of the body. The identification is generally performed in two steps. Firstly, the constitutive model is chosen. This choice is commonly made on the basis of physical intuition and *a priori* knowledge, but it can also be made by using mathematical tools. Secondly, the constitutive parameters or functions of the chosen model are determined. In Papers A - C the constitutive model is chosen *a priori*, and only the second step of the identification is considered, while in Paper D the complete identification problem is treated.

There is great need of methods which are convenient to use in a routine manner for the identification of viscoelastic materials. Here impact is used as means of excitation. This excitation has the advantage of requiring simple devices, such as those in Papers A and B. Furthermore, impact gives excitation within a wide frequency range of interest to mechanical and acoustical engineers. A disadvantage is that it may be difficult to control the distribution of energy over the frequency range. Often used alternatives to the impact excitation is harmonic and noise excitation by means of an

electromagnetic exciter. In order to obtain experimental procedures which are easily realizable, and to obtain mathematical simplicity, it is desirable that the geometry of the test specimens be simple. Therefore, slender rods are used in Papers A - D, something which permits the use of one-dimensional theory.

The mechanical behaviour of polymers is generally nonlinear. If, however, the levels of stresses and strains are low it is reasonable to use linear constitutive models. Papers A and B concern linear and Papers C and D nonlinear viscoelastic models.

The force between two impacting bodies is typically of short duration and of large amplitude. This circumstance is used in, e. g., percussive drilling where impacts are used to break hard materials such as rock and concrete. In other cases the large forces are undesired and may cause severe damage. There is often need of determining or predicting the time history of the impact force. The latter task may demand large computational effort, and it requires complete knowledge of the geometries and the materials of the impacting bodies. The material properties may be determined through identification procedures like, e. g., those in Papers A - D. In contrast, a method for prediction of impact force is established in Paper E, where the bodies are characterised dynamically through a routine impact test on each of the two bodies, and where data from these tests allow simple determination of the impact force. A prerequisite is that the bodies behave linearly in the impact process.

In Section 2 of this survey some fundamentals of one-dimensional theory of wave propagation in viscoelastic rods are given. This theory is employed in the five papers of this thesis. Furthermore, the two principal constitutive models used to describe the dynamic viscoelastic properties are given. In Section 3 the methods of Papers A and B for identification of linear viscoelastic materials are presented with some typical results from the experimental tests and with the application of Paper C. In Section 4 the method of Paper D for identification of nonlinear viscoelastic materials is presented. In Section 5 the method of Paper E for prediction of impact force is presented. In Section 6, finally, some conclusions are made.

EXTENSIONAL WAVES IN VISCOELASTIC RODS

The propagation of extensional waves in a rod is generally influenced by three-dimensional effects. If the rod is straight and slender and the transverse dimension of the rod is much smaller than the shortest characteristic length of the waves, then three-dimensional effects can be neglected. Under such conditions the propagation of extensional waves in the rod may be represented by the system of partial differential equations

$$\frac{\partial \sigma}{\partial x} = \rho \frac{\partial v}{\partial t} \quad (2.1)$$

$$\frac{\partial \epsilon}{\partial t} = \frac{\partial v}{\partial x} \quad (2.2)$$

$$\Phi \left(\sigma, \epsilon, \frac{\partial \sigma}{\partial t}, \frac{\partial \epsilon}{\partial t}, \dots \right) = 0 \quad (2.3)$$

where x is an axial coordinate, t is time, $\sigma(x,t)$ is the normal stress, $v(x,t)$ is the particle velocity, $\epsilon(x,t)$ is the normal strain, and ρ is the density. Relation (2.1) is the equation of motion and equation (2.2) expresses compatibility. Equation (2.3) is the constitutive relation of the material of the rod. In order to solve these equations one has to specify the constitutive relation and add appropriate boundary and initial conditions.

In the case of a general linear viscoelastic material the constitutive relation can be expressed

$$\hat{\sigma} - E \hat{\epsilon} = 0, \quad (2.4)$$

where the circumflex accent denotes Fourier transformation. This constitutive model is employed in Papers A, B, C and E. The function $E = E' + iE''$ of frequency ω is the complex modulus. In the case of a linear elastic

material E is Young's modulus, which is independent of frequency, and relation (2.4) reduces to Hooke's law $\sigma-E\epsilon=0$.

Another constitutive relation for a viscoelastic material, used in Paper D, is

$$\frac{1}{E_0} \frac{\partial \sigma}{\partial t} + F(\sigma) - \frac{\partial \epsilon}{\partial t} = 0 \quad (2.5)$$

for a Maxwell model. Here E_0 is the Young's modulus, which characterizes the elastic part of the strain rate, and $F(\sigma)$ is a constitutive function which represents the inelastic part of the strain rate. The function $F(\sigma)$ can, as in Paper D, be linear or nonlinear.

IDENTIFICATION OF LINEAR VISCOELASTIC MATERIALS

Different methods have been proposed for determination of the complex modulus in different frequency ranges. At low frequencies, where the wavelength is much longer than the dimensions of the specimen, it can be determined in a quasi-static test. At higher frequencies, however, the effects of wave propagation have to be taken into account. For the approximate frequency range 20 - 20 000 Hz, a common way is to perform measurements on excited rods. This was first done on vibrated rods by Norris and Young [1], and on impacted rods by Blanc [2]. Several papers [3 - 5] have been published on further developments of their methods. It has been found [1, 5] that accelerometers are often well suited gauges for this kind of measurements. Furthermore, as mentioned in the introduction, impact is a simple means of wide-band excitation.

In Paper A a method is presented where accelerometers and impact excitation are used to determine the complex modulus. It is sometime desired to determine the complex modulus of a material which serves in a structure. Therefore there is need of methods which permit the determination *in-situ* of the complex modulus. In Paper B such a method is proposed.

3.1 Theory

Consider a rod on which the end-point accelerations are measured by means of accelerometers with masses m . The length of the rod is L , the cross-sectional area is A , and the density is ρ . The rod is given a slight impact at one end as illustrated in Figure 3.1.

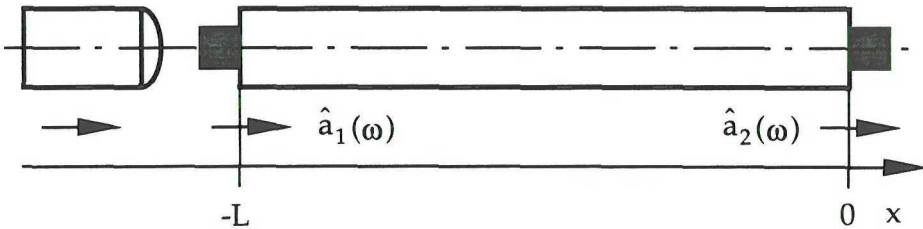


Figure 3.1. Impacted rod specimen of linear viscoelastic material with accelerometers attached to its end.

If relation (2.4) is taken as the constitutive law of the material it is shown in Paper A, that the complex modulus E is related to the end-point accelerations through the equation

$$\cosh(\gamma L) + \mu\gamma L \sinh(\gamma L) = \Psi \quad (3.1)$$

where $\gamma^2 = -\rho\omega^2/E$ is the square of the wave propagation coefficient, $\mu = m/AL\rho$ is the ratio of the accelerometer mass to the rod mass, and $\Psi = \hat{a}_1/\hat{a}_2$ is the complex acceleration ratio. This equation was first established by Norris and Young [1] for the case of harmonic excitation. It has an infinite number of solutions for E , one of which is the physically relevant. No exact solution has been presented in the literature except in the case $\mu = 0$ [3], i. e., in the case of a massless accelerometer. In Paper A the relevant solution is obtained by means of an iterative procedure. An approximate solution for small μ , based on the above exact solution, is proposed as well. The method will be referred to here as the two-point method.

In the method described above, the complex modulus E is determined from the end-point accelerations and from knowledge of the boundary condition at the non-impacted end. Consider now instead a case where the boundary conditions at both ends are unknown. The rod may, e. g., be a member of a structure with unknown properties. In Paper B it is shown that the complex modulus E can be determined if the structure is impacted and the strains are measured at three equidistant sections of the rod member, as shown in Figure 3.2. The method proposed in Paper B can therefore be used for *in-situ* determination of the complex modulus.

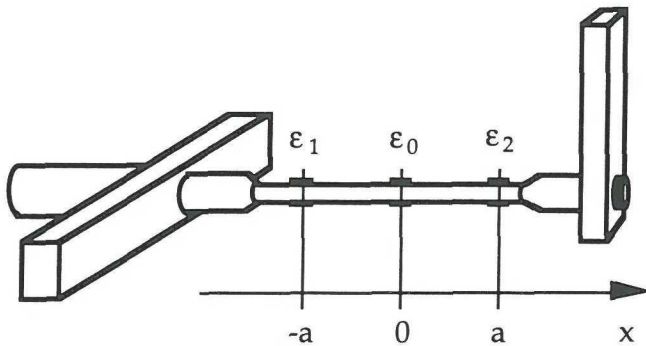


Figure 3.2. Instrumented linear viscoelastic member of a structure.

In this case the relation between the complex modulus and the measured quantities is

$$\cosh(\gamma L) = \Psi. \quad (3.2)$$

Here Ψ is defined by $\Psi = (1/2)(\hat{\epsilon}_1 + \hat{\epsilon}_2)/\hat{\epsilon}_0$. In Paper B this equation is solved analytically for E by using the solution found by Lundberg and Blanc [3]. The *in-situ* method will be referred to here as the three-point method.

3.2 Experiments and results

The two methods for identification of complex modulus presented above have been tested experimentally and the complex modulus has been identified for two polymers, viz., polypropylene and polyamide 6. The two-point method was tested on rod specimens of various lengths between 200 and 800 mm and of diameter between 11 and 19 mm. Light-weight high-frequency accelerometers were used. The three-point method was applied to a 800 mm polypropylene rod mounted in a simple structure, and semiconductor strain gauges were used. In order to obtain a slight impact a small pendulum steel hammer was used in all the tests. In Figure 3.3 some typical results, obtained for polypropylene using the two methods presented above, are shown and compared to results obtained using the method of Blanc [2]. The results agree well even though the results obtained with the three-point method are afflicted with larger scatter in the imaginary part of the

complex modulus. In Paper A there are further results which show that this scatter increases with decreasing damping.

The complex modulus is strongly temperature dependent. Therefore, the complex modulus was determined at elevated temperatures as well as at ambient temperature. This was done, as described in Paper A, simply by putting the instrumented specimen and the pendulum in an oven. Complete results together with the experimental details of the two methods are given in Papers A and B.

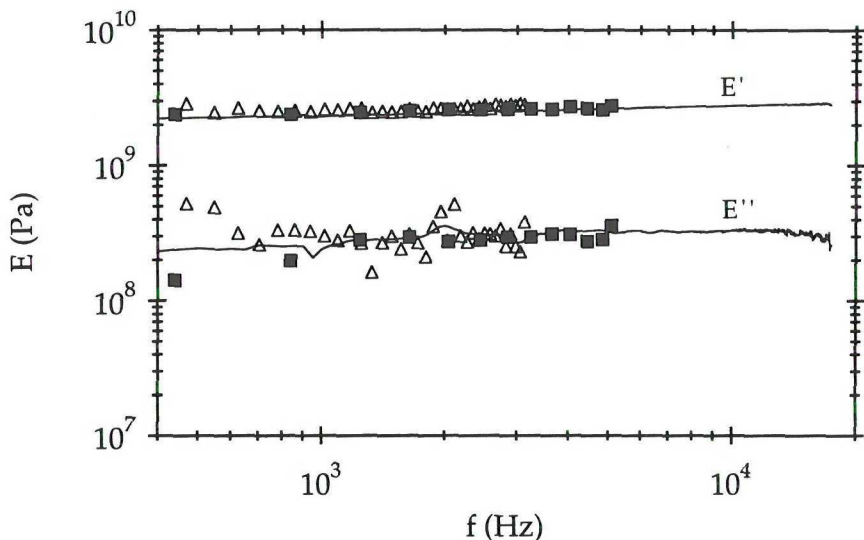


Figure 3.3. Complex modulus $E = E' + iE''$ for polypropylene versus frequency f . Comparison is made between results obtained using the two-point method (—), the three-point method (Δ) and the method developed by Blanc (■).

The frequency range in which the results from the two- and three-point methods can be considered valid is bounded upward by the use of the one-dimensional model. Furthermore, in practice the excitation also puts an upper limit on the useful frequency range. The lower limit is determined by the restriction that the wavelength should not be too long compared to the distance between the gauges. In Paper A it is shown that, with these restrictions taken into account, the two-point method yields useful results

in a frequency range of approximately two decades. The corresponding frequency range for the three-point method was narrower due to poorer excitation of the higher frequencies and due to a smaller distance between the gauges

3.3 Complex modulus during creep recovery

As an application of the two-point method the complex modulus of polyoximethylene during creep recovery has been investigated. It is known that the complex modulus of many polymers undergoes transient changes during creep. It has been suggested that this could be taken into account by means of nonlinear constitutive models [6]. In this case the complex modulus is defined as the differential (tangential) complex modulus for small perturbations of dynamic strains superimposed on the static strains. The complex modulus may change rapidly, especially immediately after the loading or unloading. Therefore, there is need of methods for determination of the complex modulus which are rapid and induces only a small perturbation on the test specimen. The two-point method of Paper A fulfil these requirements.

In Paper C this method was used to determine the complex modulus of polyoximethylene during creep recovery. Test were performed on rod specimens with creep loads of various magnitudes and durations. It was found that the loss factor $\tan\delta$, defined by $\tan\delta = E''/E'$, was considerably higher, and decreasing, during creep recovery compared to the loss factor before creep. The absolute value of the complex modulus was slightly lower, and increasing, compared to the absolute value before creep. Also, it was found that the complex modulus returned to its initial value within approximately 5 hours.

In order to describe the observed changes in the complex modulus, a simple three-element rheological model is employed in Paper C. The model consists of a linear spring with elastic modulus E_1 , in parallel with a nonlinear dashpot with viscosity η , which in turn are connected in series to a linear spring with elastic modulus E_2 . Here η is the differential viscosity defined by $\eta = d\sigma/d\dot{\epsilon}$ where σ and $\dot{\epsilon}$ are the stress and the strain rate of the dashpot, respectively. As the dashpot is nonlinear and, consequently, η is a function of the stress over the dashpot, the complex modulus obtained with

this model changes during creep recovery. The Norton power-law is adopted according to which the differential viscosity can be expressed as

$$\eta = 1/[B(m+1)|\sigma|^m] \quad (3.3)$$

This model has four constitutive parameters to be determined: The elastic moduli E_1 and E_2 , and B and m . The determination of the parameters was done by fitting the results obtained from the model to those from the experiments. In Figure 3.4 results for the loss factor $\tan\delta$ at the frequency of 10 kHz are shown. They are given in terms of the time-dependent part $\Delta\tan\delta$ of the loss factor, and the loss factor $\tan\delta_0$ for the unstrained material. Details and more results are given in Paper C.

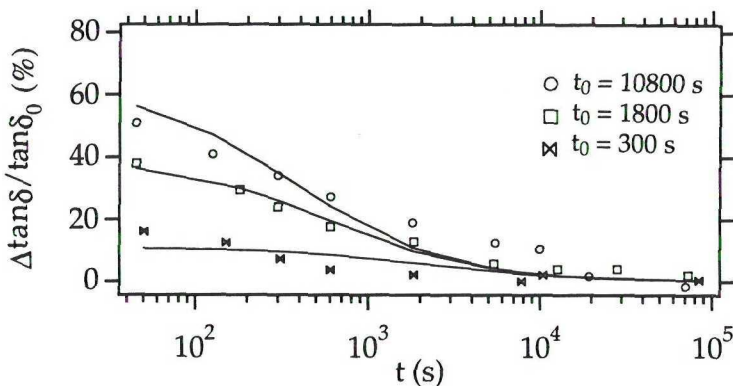


Figure 3.4. Results from tests with creep stress 32 MPa and duration t_0 . Symbols indicate measured values. Continuous lines give corresponding theoretical results obtained by using the three-element model.

3.4 Concluding remarks

In this section two methods for determination of complex modulus have been proposed and tested experimentally. The two-point method presented in Paper A was found to give accurate results in a frequency range of two decades for materials with a damping which is not too low. For low-loss materials the determination of the imaginary part of the complex modulus

is less accurate. An advantage of the two-point method is its experimental simplicity. The three-point method proposed in Paper B provides a means for *in-situ* determination of the complex modulus. This is interesting if, e.g., one wants to determine the complex modulus of an aging material which serves in a structure. The results obtained with the three-point method are less accurate than those obtained with the two-point method. Nevertheless, the method for determination of the complex modulus *in situ* is meant to be of a practical value. In Paper C, finally, the two-point method is applied to determine the complex modulus of polyoximethylene during creep recovery. The proposed nonlinear rheological model gives a qualitatively good description of the changes in the loss factor. The model also predicts changes in the absolute value of the complex modulus. However, those changes are much smaller than the observed ones.

IDENTIFICATION OF NONLINEAR VISCOELASTIC MATERIALS

In Paper D the possibilities of determining viscoelastic properties from measurements on an impacted rod specimen are further utilized. Nonlinear as well as linear constitutive relations are considered. Furthermore, the complete identification problem is solved, i. e., both the choice of the constitutive model and the determination of the parameters of that model. In Paper D these procedures are referred to as *model identification* and *parameter identification*, respectively. Finally, a device for contactless measurement of displacements was used.

One of the classical viscoelastic models is the Maxwell model [7]. The original Maxwell model was linear but it can easily be extended to cope with nonlinear behaviour by changing one or both of its linear elements into nonlinear ones, e. g., as in Paper D, by choosing the function F in equation (2.5) to be nonlinear.

4.1 Theory

Consider a rod on which the particle velocity is measured at two sections. The rod is impacted at one end as illustrated in Figure 4.1.

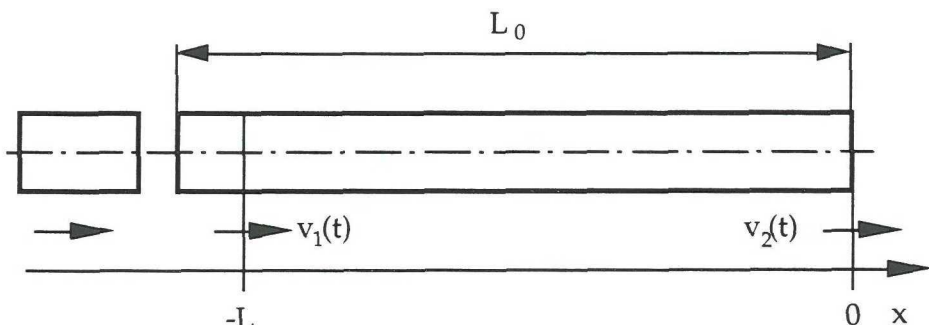


Figure 4.1. Projectile and rod specimen.

Suppose that expression (2.5), corresponding to the Maxwell model, is taken as the constitutive relation for the material. The identification problem is in this case formulated as follows: Given the two velocities $v_1(t)$ and $v_2(t)$ and the length L , determine the constitutive function $F(\sigma)$ and the elastic modulus E_0 . In Paper D this problem is solved in two steps: (i) The model identification, where the form of the function $F(\sigma)$ is chosen, and (ii) the parameter identification, where E_0 and the parameters of the chosen constitutive function are determined.

The model identification is performed using pattern recognition theory [8]. The constitutive function $F(\sigma)$ is chosen among the following alternatives:

$$F_1 = \sigma/\eta$$

$$F_2 = |\sigma|^k \operatorname{sgn}(\sigma)/B \quad (4.1)$$

$$F_3 = \sigma \exp(|\sigma|/m)/\eta.$$

The first function corresponds to the linear Maxwell model. The second and third functions correspond to the Maxwell-Norton model and the Maxwell-Gurevitch-Rabinovitch model [9], respectively. The first step of the model identification procedure is to form a large number of standard samples. They are formed by introducing a large number, in Paper D approximately 60, of sets of parameter values for each of the three models above. Then a simulated velocity $v_2(t)$ is obtained for each set of parameter values by solving equations (2.1, 2.2, 2.5) with the actual boundary and initial conditions, and with the velocity $v(t,-L)$ equal to the measured velocity $v_1(t)$. Finally, these simulated velocities $v_2(t)$ are compared to the corresponding measured velocity in the same experiment using a stochastic classifier [10]. This yields measures P_i , $i = 1, 2, 3$, of the adequacy of the model involving the function F_i for representation of the material behaviour. These quantities have the property $0 < P_i < 1$, where a high value of P_i indicates high adequacy. The model corresponding to the highest adequacy is then chosen to represent the material. The principal steps of the model identification are outlined in Paper D, and the details are given in [11].

The problem of parameter identification is solved by minimizing the difference between the simulated velocity $v_2(t)$ and the corresponding measured velocity. In Paper D this is done by using a least-square method

[12] which is the natural choice when there is no information available on noise in the data.

4.2 Experiments and results

The method for identification of nonlinear viscoelastic materials outlined above have been tested experimentally on five polymers, viz. polypropylene, polyamide 6, polyoximethylene, polyethylene and a carbon-black filled natural rubber. Tests were performed on rod specimens with lengths between 200 and 800 mm and diameters between 12 and 17 mm. Electro-optical transducers were employed for contactless measurement of the displacements u_1 and u_2 , from which the velocities v_1 and v_2 were obtained by numerical differentiation. In order to obtain nonlinear behaviour, considerably more powerful impacts had to be used as excitation, compared to those used in Papers A - C. Therefore, a small spring-driven gun was used to generate impacts with impact velocities of approximately 10 m/s.

The results obtained are exemplified here by those for polypropylene: The adequacy measures P_i obtained for the three models considered were $P_1 = 0.220$, $P_2 = 0.712$ and $P_3 = 0.106$, respectively. Consequently, the model with the constitutive function F_2 was chosen as the most adequate one and was used in the parameter identification procedure. The identified parameters were $E = 2.580 \text{ GPa}$, $\kappa = 2.108$ and $B = 38.16 \text{ EPa}^\kappa \text{s}$. A detailed description of the experiments and complete results are given in Paper D.

4.3 Concluding remarks

In this section, corresponding to Paper D, a method for identification of nonlinear viscoelastic materials has been presented. The identification was performed on the basis of displacement measurements on an impacted rod specimen. Due to the use of electro-optical transducers, the experimental procedure was simple and could be carried out by routine. In Paper D it was found that, when introducing data from several tests on specimens with different lengths into the parameter identification procedure, the deviation between simulated and measured velocities v_2 remained approximately constant and at a low level for all tested materials. This confirms that the

constitutive model chosen for each material in the model identification is suitable for representing the behaviour of the material under load conditions similar to those in the experiments on which the identification was based.

PREDICTION OF IMPACT FORCE

The force generated between two impacting bodies can be determined either by measurement or by prediction. The former is dependent on data obtained during impact while the latter is not. Such data can be captured by a force transducer placed between the bodies [13, 14] or by gauges attached to one of the impacting bodies [15, 16]. Predictions of impact force are generally based on data for the materials, such as those obtained in Paper A - D, on the geometries of the impacting bodies, and on the impact velocity in conjunction with an impact model. Such general treatments of the impact problem commonly give more information than the impact force, and considerable computational efforts may have to be spent. In Paper E a method is established for the prediction of impact force between bodies made of linearly elastic or linearly viscoelastic materials. Each impacting body is characterized by its impulse response. This characterization is specific to the impact problem at hand. As a result, only limited computational efforts have to be spent to predict the impact force.

5.1 Theory

Consider two impacting bodies made of linearly elastic or linearly viscoelastic materials, as shown in Figure 5.1. It is assumed that the impact interface can be attributed a single velocity and that this velocity is parallel to the impact velocity V . Furthermore, it is presumed that the problem is linear. This presumption is fulfilled if the deformations are small, if the area of the interface is constant during the impact, and if there is no combined effects of friction and slip. The bodies are characterized by their impulse responses $G_1(t)$ and $G_2(t)$ defined by the convolutions

$$v_i(t) = G_i(t) * F_i(t), \quad i = 1, 2. \quad (5.1)$$

Here $F_i(t)$ is a force, positive in compression, acting on the impact face of body "i", and $v_i(t)$ is the velocity of the same impact face.

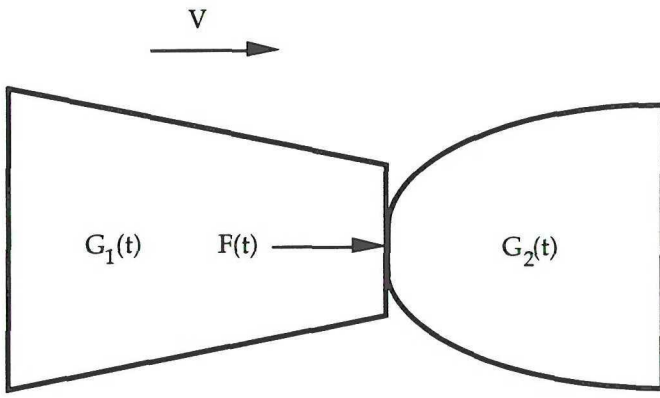


Figure 5.1. Impact between bodies with impulse responses $G_1(t)$ and $G_2(t)$.
The impact velocity is V and the impact force $F(t)$.

Before contact is established at time $t = 0$, the first body has the impact velocity V and the second is at rest. Both bodies are unstressed. Provisionally it is assumed that the impact faces stick to each other for $t \geq 0$. Therefore they have the same velocity. They interact with a force $F_s(t)$, positive in compression, which satisfies the integral equation [17]

$$[G_1(t) + G_2(t)] * F_s(t) = VH(t) \quad (5.2)$$

where $H(t)$ is Heaviside's unit step function. It is obvious that the force $F_s(t)$ is initially positive. Due to the assumption that the impact faces stick to each other, $F_s(t)$ may, however, become negative at some time $t = t_0$. The physical interpretation of this is that the bodies rebound, and that the impact ends. In such a case the impact force $F(t)$ is given by

$$F(t) = F_s(t)[H(t) - H(t-t_0)], \quad (5.3)$$

where $H(t)$ is the Heaviside's step function. Otherwise $F(t)$ equals $F_s(t)$.

Once the impulse responses $G_1(t)$ and $G_2(t)$ and the impact velocity V are known the impact force can be determined from equations (5.2) and (5.3). There are several techniques to solve the integral equations above, i. e., to perform the deconvolutions. In Paper E this is done in the frequency domain, where convolutions transform into multiplications, using continuous and discrete Fourier transforms. This is a technique which can

be used, e. g., when there is energy dissipation in at least one of the bodies. However, it can not be used when both bodies are elastic and finite. A related more general technique which makes use of Laplace transforms is presented in [16].

In principle there are two ways of determining the impulse responses of the impacting bodies. The impulse responses can be determined by measuring the velocity $v_i(t)$ and the force $F_i(t)$, and then solving the integral equation (5.1) numerically. They can also be predicted by solving the boundary and initial value problem for the body at hand.

5.2 Experiments and results

In Paper E the impulse response method was tested with three objects: A truncated cone made of polyamide 6 with length 400 mm and maximum diameter 75 mm, a compound cylinder made of aluminium and polyamide 6 with length 500 mm and diameter 32 mm, and a long slender rod made of steel with length 6150 mm and diameter 10 mm. The impulse responses were determined through measurements by means of an impedance head mounted on the impact face. An impedance head is a combined accelerometer and force transducer. Thus, it can measure simultaneously the force F_i and the acceleration a_i . The acceleration was integrated numerically in order to give the required velocity v_i . The impedance head was given a slight impact by a small pendulum steel hammer. The impulse responses were also predicted using the one-dimensional theory outlined in Section 2. The viscoelastic model (2.4) was used for polyamide 6 and data were taken from experimental tests [3] in which a method related to that of Paper A was employed. The steel rod and the aluminium parts of the cylinder were considered linearly elastic.

Finally, the impact force was predicted from equations (5.2) and (5.3) with different combinations of the measured and predicted impulse responses of the three test objects. The predicted impacted forces were compared to those measured in impact tests in which the steel rod was instrumented with strain gauges. The predicted and measured impact forces are shown in Figure 5.2 for the case of impact between the compound cylinder and the steel rod. The experimental set-ups as well as complete results are given in Paper E.

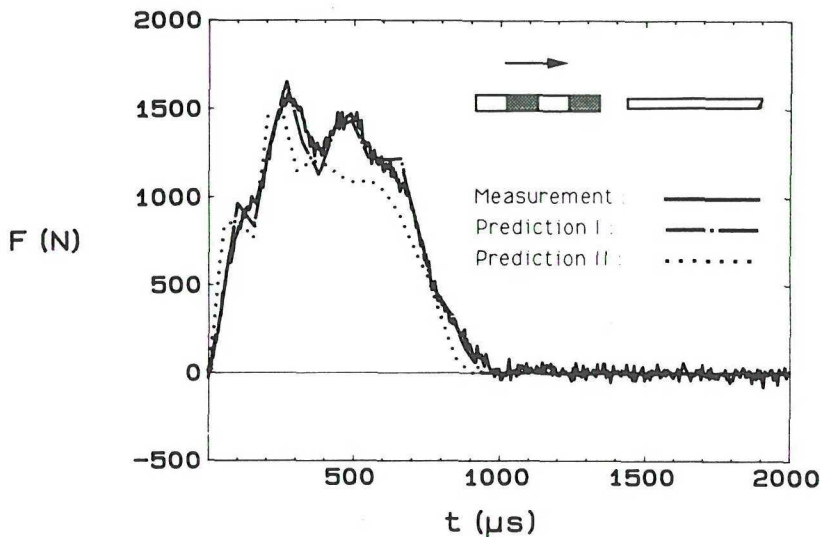


Figure 5.2. Measured and predicted impact force F versus time t for impact between the compound cylinder and the steel rod. The predictions are based on impulse responses which are (I) measured for the cylinder and predicted for the rod, and (II) predicted for both bodies

5.3 Concluding remarks

In this section, corresponding to Paper E, a method has been presented for prediction of impact force based on the impulse responses of the impacting bodies. The impulse responses serve to characterize the impacting bodies in a specific way adopted to the impact problem at hand. Impact forces have been predicted using both measured and predicted impulse responses. The predictions of impulse responses were made according to the one-dimensional theory outlined in Section 2. The impact forces predicted have been compared to those measured in impact tests. Generally, the predictions based on measured impulse responses agree better with the measurements than the predictions based on predicted impulse responses. This is explained mainly by the three-dimensional behaviour of the bodies which is taken into account in the measured impulse responses but not in the predicted ones. Nevertheless, the one-dimensional theory gives fairly good results.

CONCLUSIONS

In this thesis methods for identification of viscoelastic materials and for prediction of impact force have been proposed, which are easily realized experimentally. The methods are based on measurements on impacted bodies.

In Sections 3 and 4 measured responses of impacted rod specimens and rod-like members of impacted structures were used to identify linear and nonlinear viscoelastic materials. In Paper A it was shown that the complex modulus can be determined, in a frequency range of approximately two decades, from measured end-point accelerations of an impacted rod specimen. The method has been tested on two polymers, and it was found to be convenient to use at elevated temperatures as well as at room temperature. The method should be suitable for fast routine testing of materials, provided that the damping of the material is not too low. In Paper B an *in-situ* method for determination of complex modulus was proposed. It was shown that if strains are measured at three sections of a rod-like member of an impacted structure, the complex modulus can be determined from these strains without knowledge about the other parts of the structure. In Paper C the method of Paper A was applied to determine the complex modulus of polyoximethylene during creep recovery. It was shown that the changes in the loss factor can be accounted for by means of a simple nonlinear constitutive model. In Paper D displacements measured at two sections of an impacted rod specimen were used to identify nonlinear viscoelastic materials. It was shown that the constitutive model can be chosen by using pattern recognition theory, and that the parameters of the chosen model can be identified by using a least-square method. Electro-optical transducers were used for contactless measurement of the displacements. Therefore the test specimens required minimum preparation, which made the experimental procedure simple and fast.

In Section 5, corresponding to Paper E, it was shown that the impact force can be predicted from the velocity response of each body to an impulsive force applied to its impact face, and from the impact velocity. Measured as

well as predicted impulse responses have been used. Furthermore, when measured impulse responses are used, the experimental and computational efforts are independent of the complexity of the particular impact problem. This is a major advantage of the impulse response method.

REFERENCES

1. D. M. NORRIS JR and W. C. YOUNG, Complex modulus measurement by longitudinal vibration testing. *Experimental Mechanics* **10**, 93-96 (1970).
2. R.H. BLANC, Détermination de l'équation de comportements des corps viscoélastiques linéaires par une méthode d'impulsion. *Doctoral Thesis, Université d'Aix-Marseille* (1971).
3. B. LUNDBERG and R. H. BLANC, Determination of mechanical material properties from the two-point response of an impacted linearly viscoelastic rod specimen. *Journal of Sound and Vibration* **126**, 97-108 (1988).
4. J. L. BUCHANAN, Numerical solution for the dynamic moduli of a viscoelastic bar. *The Journal of the Acoustical Society of America* **81**, 1775-1786 (1987).
5. T. PRITZ, Transfer function method for investigating the complex modulus acoustical materials: Rod-like specimen. *Journal of Sound and Vibration* **81**, 359-376 (1982).
6. J. OTHMEZOURI-DECERF, Interpretation of the mechanical damping behaviour of glassy polycarbonate strained in the non-linear range of deformation below the yield point. *Polymer* **29**, 641-645 (1988).
7. R.M. CHRISTENSEN, *Theory of viscoelasticity. An introduction*, Second ed., Acad. Press (1982).
8. G. MAIER, F. GIANESSI and A.NAPPI, Indirect identification of yield limits by mathematical programming. *Eng.Struct.* **4**, 86-98 (1982).
9. N. CRISTESCU and I. SULICIU, *Viscoplasticity*, Martinus Nijhoff Publishers (1982).
10. J. TOU and R. GONZALEZ, *Pattern recognition principles*. Addison-Wesley Publ. Comp. (1974).
11. I. N. TRENDAFILOVA, On a method for mechanical-mathematical model identification using a stochastic pattern recognition approach. *European Journal of Mechanics A-Solids* **11**, 767-779 (1992).
12. P. EYKHOFF, *System identification*. J.Wiley & Sons (1974).

13. S. TANIMURA, A new method for measuring impulsive force at contact parts. *Experimental Mechanics* **24**, 271-276 (1984).
14. K. G. SUNDIN and M. JONSSON, A stiff and compact force transducer based on strain measurement. *Experimental Mechanics* **25**, 48-53 (1985).
15. B. LUNDBERG and A. HENCHOZ, Analysis of elastic waves from two-point measurement. *Experimental Mechanics* **17**, 213-218 (1977).
16. H. INOUE, R. WATANABE, T. SHIBUYA and T. KOIZUMI Measurement of impact force the by deconvolution method. *Transactions of the JSNDI* **2**, 63-73 (1989).
17. B. LUNDBERG and M. LESSER, On impactor synthesis. *Journal of Sound and Vibration* **58**, 5-14 (1978).

A

DETERMINATION OF COMPLEX MODULUS FROM MEASURED END-POINT ACCELERATIONS OF AN IMPACTED ROD SPECIMEN

S. ÖDEEN AND B. LUNDBERG

Department of Mechanical Engineering, Luleå University of Technology
S-951 87 Luleå, Sweden

Abstract - A method is presented for determination of the complex modulus of a linearly viscoelastic material from measured end-point accelerations of an impact-loaded rod specimen. An iterative numerical scheme was used. An approximate analytical solution was also established for the case of small accelerometer mass relative to the specimen mass. Tests were carried out at room temperature for polypropylene, with relatively high losses, and polyamide 6, with relatively low losses. Tests were also performed at temperatures between 20 and 140 °C for the former material. Valid results were obtained in the approximate frequency range of 400 Hz to 20 kHz with specimen diameters between 11 and 21 mm, and specimen lengths between 200 and 800 mm. For polypropylene these results are in good agreement with those obtained using a different method developed by Blanc. For polyamide 6, however, there was some disagreement for the imaginary part of the complex modulus. The method was convenient to use at elevated temperatures as well as at room temperature. It should be suitable for fast routine testing of materials provided that the losses are not too low.

1. INTRODUCTION

Knowledge of the complex modulus is a prerequisite for an efficient use of viscoelastic materials in dynamically loaded structures. Therefore there is need of testing methods which are convenient to use in a routine manner at elevated temperatures as well as at room temperature.

The complex modulus can be determined from the response of a rod specimen subjected to different kinds of dynamic loads. Thus, for example, a specimen can be loaded harmonically at one end and accelerations can be measured at both ends. From these accelerations the complex modulus can be evaluated at resonant frequencies according to Norris and Young [1] and Madigosky and Lee [2], and at non-resonant frequencies according to Pritz [3]. The complex modulus can also be determined using white-noise load, as

shown by Beda [4]. Error analysis was carried out by Buchanan [5], who also solved the identification problem numerically.

Alternatively, the complex modulus can be determined by measuring the transient response of an impact-loaded rod specimen. Originally, this method was restricted to such conditions that quantities associated with waves travelling in different directions could be measured separately [6-9]. This restriction was removed by Lundberg and Blanc [10], who developed a method based on strain measurements at two different cross-sections of the impacted specimen. They also solved the identification problem analytically for a specimen with a free end.

This paper presents a method which is related to the methods of Norris and Young [1], Madigosky and Lee [2], Pritz [3], and Beda [4], through the use of accelerometers, and to that by Lundberg and Blanc [10], through the use of impact excitation. Accelerometers are sensitive and can be used in wide ranges of frequency and temperature. Furthermore, impact is a fast and convenient means of providing excitation up to several tens of kilohertz at elevated temperatures as well as at room temperature.

The rod specimen was impacted at one end, and accelerations were measured at both ends. The complex modulus was determined using an iterative numerical scheme. An approximate analytical solution was also established for the case of small accelerometer mass relative to the specimen mass. In both cases use was made of analytical results obtained by Lundberg and Blanc.

The method was used for determination of the complex modulus of two polymers, viz. polypropylene and polyamide 6. For the former material, tests were performed at elevated temperatures, as well as at room temperature. The results were compared with those obtained using a different method developed by Blanc [6, 7].

2. THEORY

Consider a straight, cylindrical, slender rod specimen of linearly viscoelastic material with density ρ and complex modulus $E(\omega) = E'(\omega) + iE''(\omega)$, where ω is the radian frequency. The specimen has cross-sectional area A and length L . It is impacted axially, and accelerometers with mass m are attached to its ends as shown in Figure 1.

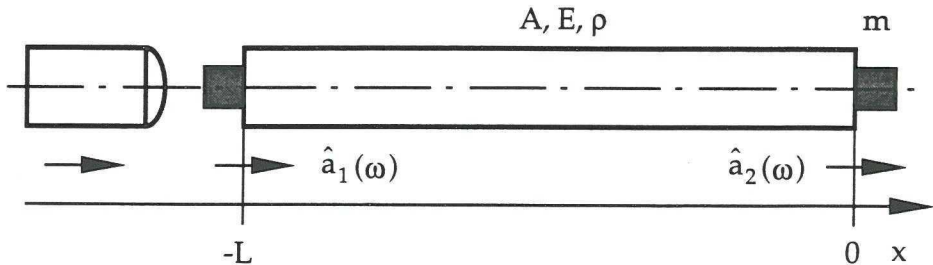


Figure 1. Impacted rod specimen of linearly viscoelastic material with accelerometers attached to its end.

With the use of one-dimensional theory, the complex modulus E can be expressed implicitly in terms of the Fourier transforms and of the endpoint accelerations through the relation

$$\cosh(\gamma L) + \mu\gamma L \sinh(\gamma L) = \Psi \quad (1)$$

where $\gamma^2 = -\rho\omega^2/E$ is the square of the wave propagation coefficient, $\mu = m/\rho AL$ is the ratio of accelerometer mass to specimen mass, and $\Psi = \hat{a}_1/\hat{a}_2$ is the complex acceleration ratio. This relation corresponds to that established by Norris and Young [1] for harmonic load. The wave propagation coefficient $\gamma(\omega)$ can be expressed $\gamma(\omega) = \alpha(\omega) + ik(\omega)$, where $\alpha(\omega)$ is the damping coefficient and $k(\omega)$ is the wave number. The real and imaginary parts of E are related to those of γ through

$$E' = \rho\omega^2(k^2 - \alpha^2)/(k^2 + \alpha^2)^2, \quad E'' = \rho\omega^2(2k\alpha)/(k^2 + \alpha^2)^2. \quad (2)$$

Equation (1) has an infinite number of complex solutions for γ . Buchanan [5] used a numerical method for finding the relevant solution. In the case $\mu = 0$, corresponding to a free specimen end, this solution can be obtained analytically in terms of $\Psi = re^{i\phi}$ using results derived by Lundberg and Blanc [10]. The result is $\gamma_0 = \alpha_0 + ik_0$, where

$$\alpha_0 = (1/L)\sinh^{-1}[(C_0 - A_0)^{1/2}], \quad k_0 = (1/L)(s\beta_0 + n\pi) \quad (3)$$

and where

$$C_0 = (A_0^2 + B_0^2)^{1/2}, \quad A_0 = (1/2)(1 - r^2), \quad B_0 = r\sin(\phi) \quad (4)$$

$$\beta_0 = \sin^{-1}[(C_0 + A_0)^{1/2}].$$

The integers $s = \pm 1$ and $n = 0, 1, 2, \dots$ are chosen according to Table 1 so that $k(\omega)$ is a continuous and monotonically increasing function with $k(0) = 0$. This solution is used below to generate numerical as well as approximate analytical solutions of equation (1) for γ .

A numerical solution can be obtained by using $\gamma_0 L$ as an initial guess in the complex Newton-Raphson iteration

$$(\gamma L)_{n+1} = (\gamma L)_n - f((\gamma L)_n)/f'((\gamma L)_n) \quad (5)$$

where $f(\gamma L) = \cosh(\gamma L) + \mu \gamma L \sinh(\gamma L) - \Psi$, and where the prime denotes differentiation with respect to the argument γL .

An approximate analytical solution, valid for small μ , can be derived by expressing the wave propagation coefficient γ as the series

$$\gamma = \gamma_0 + \gamma_1 \mu + \gamma_2 \mu^2 + \gamma_3 \mu^3 + \dots \quad (6)$$

Making Taylor series expansions of $\cosh(\gamma L)$ and $\gamma L \sinh(\gamma L)$ around $\gamma = \gamma_0$ gives

$$\gamma_1 = -\gamma_0, \quad \gamma_2 = \gamma_0 [1 + (1/2)\gamma_0 L \coth(\gamma_0 L)], \quad (7)$$

$$\gamma_3 = -\gamma_0 [1 + (3/2)\gamma_0 L \coth(\gamma_0 L) + (1/3)(\gamma_0 L)^2]$$

for the first three correction terms.

When the solution for γ has been found, numerically or analytically, the real part E' and the imaginary part E'' of the complex modulus E can be obtained from relations (2).

Table 1. Wavelength λ , phase ϕ , parameters β_0 and integers s and n versus radian frequency ω .

ω	0	\uparrow	\uparrow	\uparrow	\uparrow	\uparrow	\uparrow	\uparrow
$\lambda/4$	∞	\downarrow	a	\downarrow	$a/2$	\downarrow	$a/3$	\downarrow
$\sin(\phi)$	0		0		0		0	
$\cos(\phi)$		0		0		0		
β_0	0	$\uparrow \pi/2 \downarrow$	0	$\uparrow \pi/2 \downarrow$	0	$\uparrow \pi/2 \downarrow$	0	\uparrow
s	1	-1	1	-1	1	-1	1	
n	0		1		2		3	

3. EXPERIMENTAL TESTS

The complex moduli were determined for two materials, viz. polypropylene and polyamide 6. Cylindrical rod specimens with circular cross-sections were used. Polypropylene was tested for three specimen diameters D and three specimen lengths L, while polyamide 6 was tested for a single specimen size.

All specimens were tested at room temperature in the range $T = 21.2$ to 22.5 °C. The conditions for the room-temperature tests are given in Table 2. The polypropylene specimen used in Test 6 was also tested at temperatures between 20 and 140 °C. These tests started at 20 °C, and the temperature was increased in steps of 10 °C. The time between two consecutive tests was taken to be one hour in order to obtain a uniform temperature distribution in the specimen. The changes in the dimensions of the specimen and in the density of the material with temperature were neglected.

Table 2. Test conditions.

Test	Material	D (mm)	L (mm)	ρ (kg/m ³)	T (°C)
1	Polypropylene	10.7	199	904	21.3
2	Polypropylene	10.7	401	906	21.2
3	Polypropylene	10.6	801	903	21.3
4	Polypropylene	15.7	201	918	21.5
5	Polypropylene	15.8	400	908	21.5
6	Polypropylene	15.8	799	912	21.5
7	Polypropylene	18.8	201	918	21.5
8	Polypropylene	18.8	400	915	21.5
9	Polypropylene	18.8	800	915	21.5
10	Polyamide 6	10.7	800	1118	22.0

The experimental set-up is shown in Figure 2. The specimen was suspended in thin cords, and it was impacted axially by a pendulum steel hammer. The length of the pendulum was 210 mm, and the hammer had length 30 mm and diameter 15 mm. The mass m of the accelerometer, including the cable connector, was 2.9 g. The tests at elevated temperatures were performed in an oven (Pickstone GP450B).

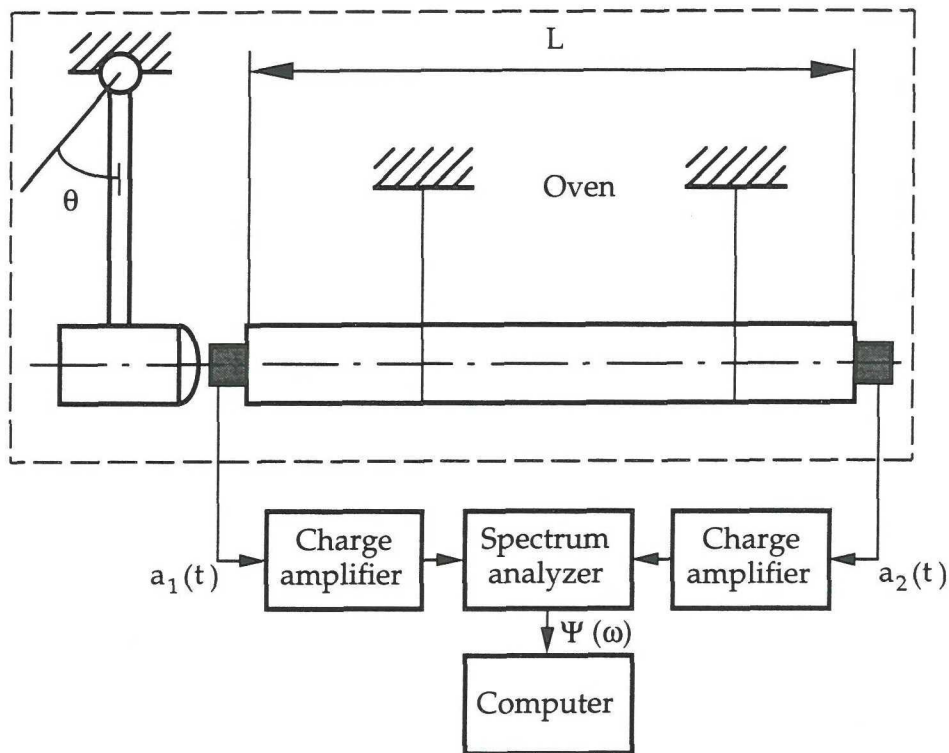


Figure 2. Experimental set-up.

The signals from the accelerometers (Brüel & Kjær 4393), representing the accelerations a_1 and a_2 , were amplified by two charge amplifiers (Brüel & Kjær 2635) and recorded by a spectrum analyzer (Tektronix 2630). The acceleration ratio Ψ was computed from ten tests as the ratio of the average cross-spectrum between a_1 and a_2 to the average auto-spectrum of a_2 . The function Ψ was transferred to a computer (Ai-Electronics PC16), and the

quantities E' and E'' were determined according to the iterative procedure (5) and the relations (2).

In order to examine the linearity of the materials, tentative tests were made with three different swing angles θ , viz. 5, 10 and 20 °. For both materials the results for 5 and 10 ° were almost identical. The swing angle of 20 °, however, gave slightly larger complex modulus, which was taken as an indication of non-linear behaviour. Therefore, the swing angle of $\theta = 10$ ° was chosen in the tests with both polypropylene and polyamide 6.

For comparison, tests were made using a different method developed by Blanc [6, 7] with the polypropylene specimen used in Test 3 and with the polyamide 6 specimen used in Test 10. The temperature and the swing angle were approximately the same as above.

4. RESULTS

Figures 3 and 4 show the results of the room-temperature tests for polypropylene and polyamide 6, respectively. Figures 5 and 6 show the results of the tests at elevated temperatures for polypropylene.

The results were considered valid, and were plotted, only if three conditions were satisfied. Firstly, the one-dimensional model used in the analysis must be sufficiently accurate. Therefore it was required that (i) the wave length $\lambda = 2\pi/k$ should exceed five times the rod diameter D . Then, according to Pritz [11], the errors in the real part E' of the complex modulus and in the loss factor E''/E' due to lateral inertia should be less than 5 per cent. Secondly, if the wave length λ is very large compared to the specimen length L , the difference between the end-point accelerations is small and, as a consequence, the results are sensitive to errors in the measurements. Therefore it was prescribed that (ii) the wave length λ should be less than five times the specimen length L . Thirdly, the iteration (5) must converge to a physically admissible solution. Therefore, it was required that (iii) the damping coefficient α and the wave number k be positive.

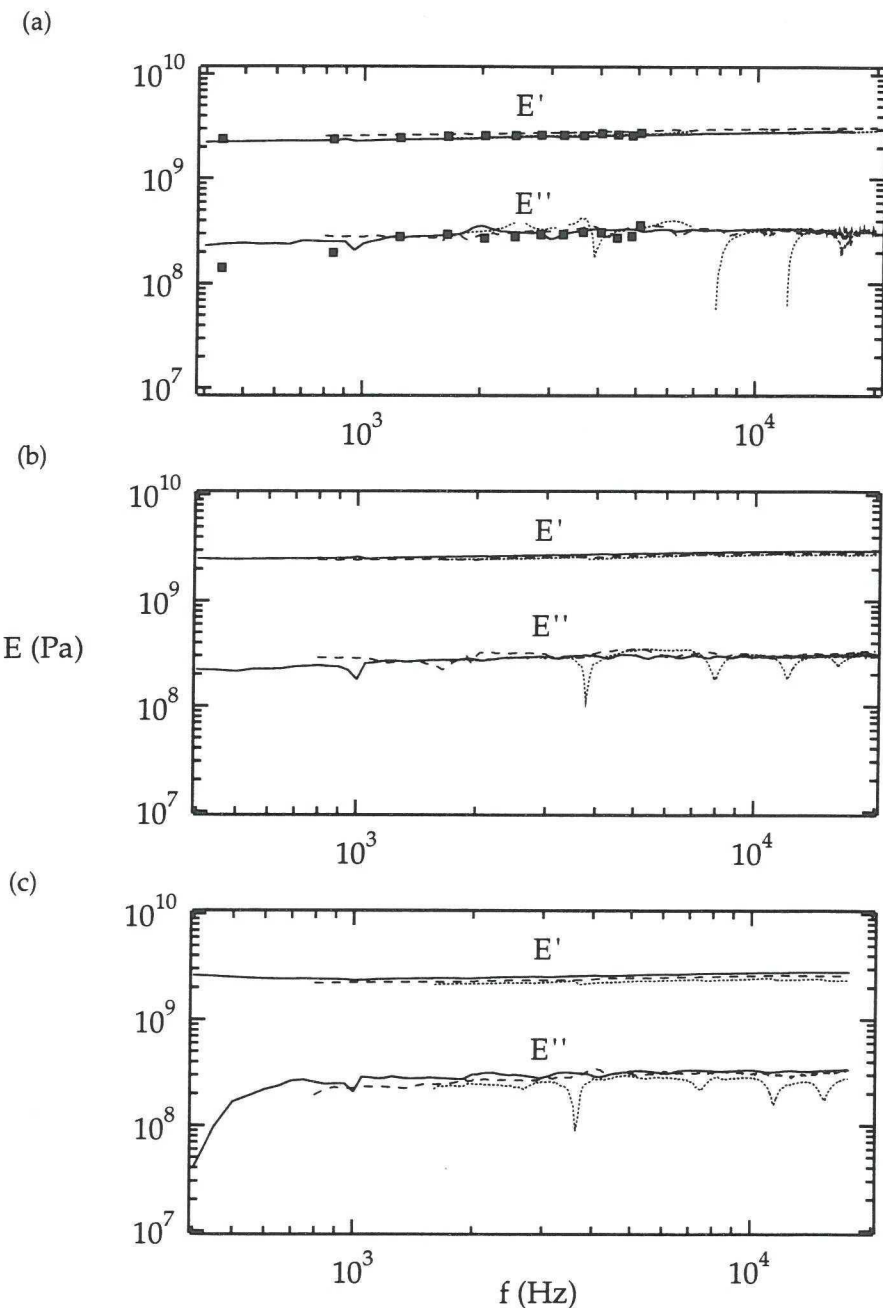


Figure 3. Complex modulus $E = E' + iE''$ versus frequency f for polypropylene. The rod diameter D is (a) 11 mm (Test 1-3), (b) 16 mm (Test 4-6) and (c) 19 mm (Test 7-9). The rod length L is 200 mm (.....), 400 mm (----) and 800 mm (—). In (a) comparison is made with the results obtained using the method developed by Blanc (■).

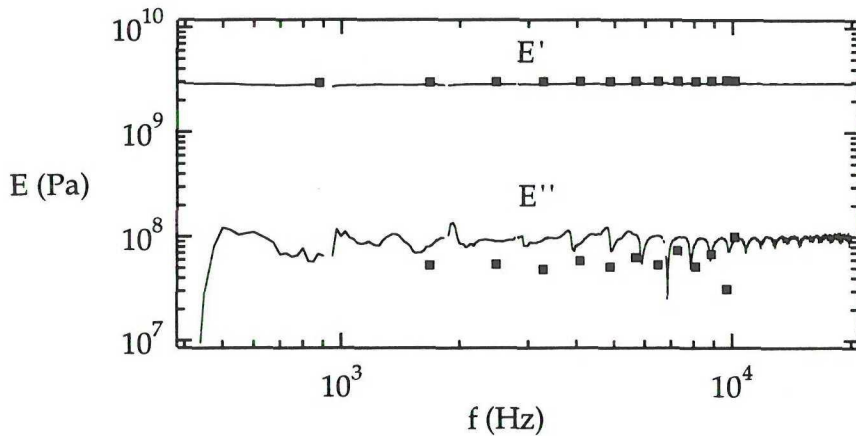


Figure 4. Complex modulus $E = E' + iE''$ versus frequency f for polyamide 6. Specimen diameter 11 mm and length 800 mm. Comparison is made between results obtained with the present method (—) and with the method developed by Blanc (■).

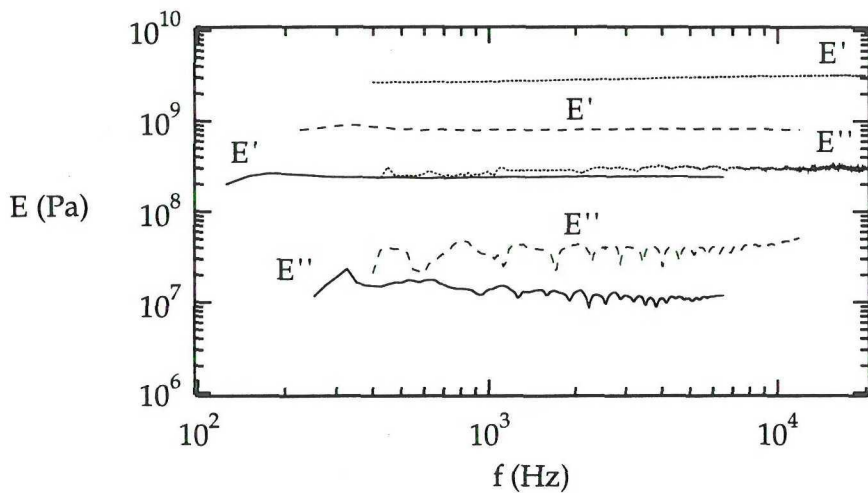


Figure 5. Complex modulus $E = E' + iE''$ versus frequency f for polypropylene at temperatures 20 °C (.....), 80 °C (- - -) and 140 °C (—).

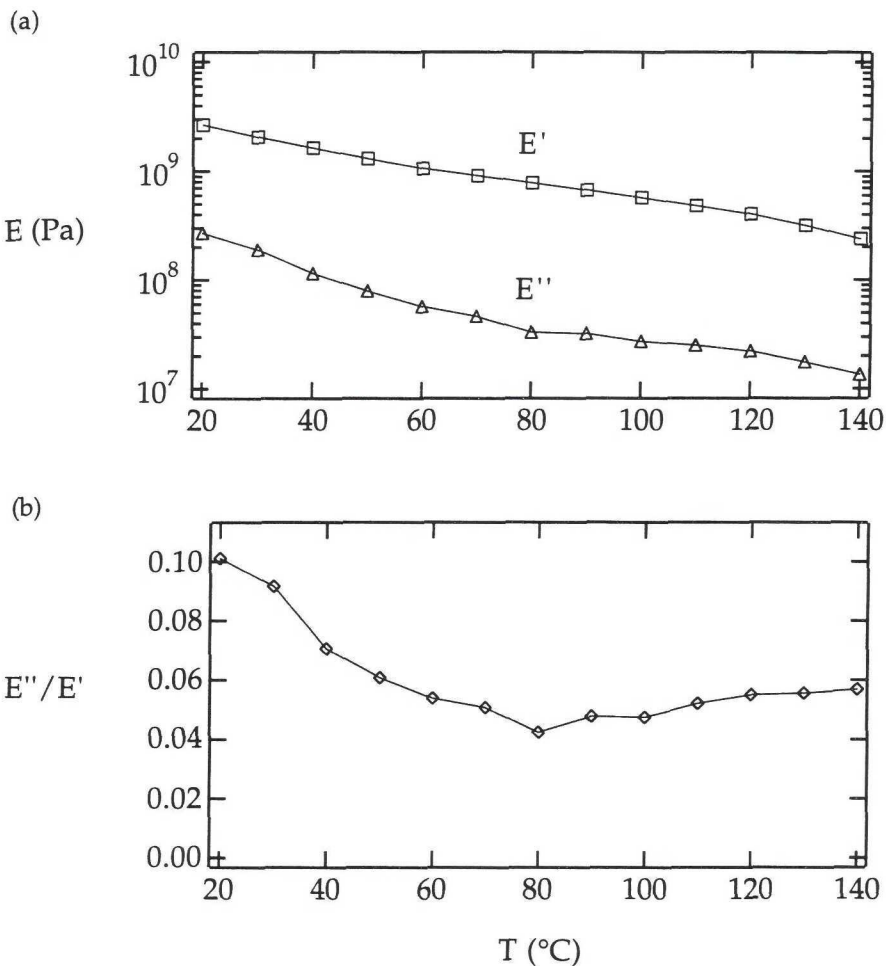


Figure 6. (a) Complex modulus $E = E' + iE''$ and (b) lossfactor E''/E' at frequency $f = 1 \text{ kHz}$ versus temperature T for polypropylene.

5. DISCUSSION

A method for determination of complex modulus from measured end-point accelerations of an impacted rod specimen has been developed. An iterative numerical scheme was employed for solving equation (1). An approximate analytical solution was also established in the case of small accelerometer mass relative to the specimen mass. Results at room temperature, such as those in Figures 3 and 4, were conveniently obtained using the numerical scheme in a frequency interval of almost two decades. Similarly, results, such as those in Figures 5 and 6, were readily obtained at elevated temperatures.

For polypropylene the results obtained using the present method agree well with those determined using the different method developed by Blanc [6, 7]. For polyamide 6, however, there is some disagreement for the imaginary part E'' of the complex modulus. Moreover, the results from tests with low-loss materials, such as polyamide 6, are afflicted with scatter in E'' . This indicates that the determination of E'' of low-loss materials is inaccurate, as is to be expected from the error analysis by Buchanan [5].

The conditions (i) and (ii) above for validity put restrictions on the specimen dimensions and the frequency range. According to condition (i) the diameter must be much smaller than the shortest wave length. From condition (ii) it follows that the specimen must not be too short relative to the longest wave length. For a given specimen, the frequency range where these conditions are satisfied is limited. Thus, these conditions give upper and lower limits, respectively, of the frequency interval. The condition (iii) was satisfied in the intervals given by conditions (i) and (ii) in all tests except Test 1, with the lightest polypropylene specimen, and Test 10, with the polyamide 6 specimen. In these two tests the iteration (5) occasionally converged to physically inadmissible solutions. For polypropylene and polyamide 6 the specimen diameters $D = 11$ or 16 mm and length $L = 800$ mm gave results in agreement with the demands in the approximate frequency range of 400 Hz to 20 kHz.

When using the approximate analytical solution, the correction terms in expression (6) should be small compared to the leading term. This essentially gives an upper limit of the frequency range. The limit frequency increases with decreasing mass ratio μ . For the tested polypropylene specimens the approximate analytical solution and the numerical solution

did not differ significantly within the frequency ranges provided by conditions (i) and (ii) when $\mu < 0.04$. A suitable requirement on an acceptable solution was found to be that the real and imaginary parts of the complex modulus determined using the first two terms in expression (6) must not differ from the corresponding quantities based on the first four terms by more than one third.

The method was convenient to use at elevated temperatures as well as at room temperature, and it should be suitable for fast routine testing of materials, e. g. in industrial environment, provided that the losses are not too low.

Acknowledgements - The Authors are in debt to the Carl Trygger Research Foundation and the Research Council of Norrbotten for their support.

REFERENCES

1. D. M. NORRIS JR and W. C. YOUNG, Complex modulus measurement by longitudinal vibration testing. *Experimental Mechanics* **10**, 93-96 (1970).
2. W. M. MADIGOSKY and G. F. LEE, Improved resonance technique for materials characterization. *The Journal of the Acoustical Society of America* **73**, 1374-1377 (1983).
3. T. PRITZ, Transfer function method for investigating the complex modulus acoustical materials: Rod-like specimen. *Journal of Sound and Vibration* **81**, 359-376 (1982).
4. T. BEDA, *Modules complexes des matériaux viscoélastiques par essais dynamiques sur tiges. Petites et grandes déformations. Modélisation, instrumentation, caractérisation*, Doctoral Thesis, Conservatoire National des Arts et Métiers de Paris (1990).
5. J. L. BUCHANAN, Numerical solution for the dynamic moduli of a viscoelastic bar. *The Journal of the Acoustical Society of America* **81**, 1775-1786 (1987).

6. R. H. BLANC, *Détermination de l'équation de comportement des corps viscoélastiques linéaires par une méthode d'impulsion* Doctoral Thesis, Université d'Aix-Marseille (1971). Published in part in *Problèmes de la rhéologie* (W. K. Nowacki, editor) 65-85 (1973), IPPT PAN, Warsaw.
7. R. H. BLANC, Progress in pulse testing methods for viscoelastic solids. *Proceedings of the 2nd National Congress on Theoretical and Applied Mechanics 1973*, Varna, Bulgarian Academy of Science Publication, Sofia, vol. 2, 555-564 (1976).
8. P. S. THEOCARIS and N. PAPADOPOLOU, Propagation of stress waves in viscoelastic media. *Polymer* **19**, 215-219 (1978).
9. Y. SOGABE, K. KISHIDA and K. NAKAGAWA, Wave propagation analysis for determining the dynamic properties of high damping alloys. *Bulletin of the Japan Society of Mechanical Engineers* **25**, 321-327 (1982).
10. B. LUNDBERG and R. H. BLANC, Determination of mechanical material properties from the two-point response of an impacted linearly viscoelastic rod specimen. *Journal of Sound and Vibration* **126**, 97-108 (1988).
11. T. PRITZ, Apparent complex Young's modulus of a longitudinally vibrating viscoelastic rod. *Journal of Sound and Vibration* **77**, 93-100 (1981).

B

IN-SITU DETERMINATION OF COMPLEX MODULUS FROM STRAIN MEASUREMENTS ON AN IMPACTED STRUCTURE

B. LUNDBERG AND S. ÖDEEN

Department of Mechanical Engineering, Luleå University of Technology
S-951 87 Luleå, Sweden

Abstract - A method is proposed for *in-situ* determination of the complex modulus of a member of an impact-loaded structure. The modulus was obtained in terms of strains measured at three different cross-sections of a uniform part of the member, using one-dimensional theory. The method was demonstrated experimentally on a cylindrical polypropylene bar mounted as a member in each of two simple frame-structures, and the modulus was obtained in the frequency range of 500 Hz to 3 kHz. For comparison, the modulus was also determined from tests on the same member, dismounted from the structures, using a different method based on measurement of end-point accelerations. The results obtained from the *in-situ* tests on the two frame-structures and from the tests on the dismounted member are in fair agreement.

1. INTRODUCTION

Viscoelastic materials, like polymers, are widely used in mechanical structures. As the mechanical properties of such materials may change due to fatigue, chemical environment, radiation, etc., it is of interest to determine these properties not only of virgin materials, but also of materials which have served in structural members.

The complex modulus can sometimes be determined for the material of a member which has been dismounted from a structure. Several methods are based on measurements on a vibrated [1-3] or impacted [4-6] uniform rod specimen. These methods require that the boundary condition be linear and known at one end.

This paper deals with the problem of determining *in situ* the complex modulus of the material of a structural member. For such a member, mounted in a structure, the boundary conditions are generally neither linear nor known. Therefore a method was proposed for which no knowledge of the boundary conditions is required.

The complex modulus was obtained in terms of strains measured at three different cross-sections of a member of an impact-loaded structure. For

simplicity it was presumed that the three instrumented cross-sections belong to a uniform part of the member. The method was demonstrated on a polypropylene bar member mounted in two simple frame-structures. The results for the complex modulus were compared with those obtained for the same member, dismounted from the structures, using a different method based on measurements of end-point accelerations [6].

2. THEORY

Consider a structure with a member, a part of which is straight, cylindrical, and made of linearly viscoelastic material. The complex modulus and the density of the material are $E(\omega) = E'(\omega) + iE''(\omega)$ and ρ , respectively, where ω is the radian frequency. The rest of the structure need not be known, and it may include any physical or geometrical nonlinearities. The uniform part of the structural member is instrumented with pairs of strain gauges at three different cross-sections as shown in Figure 1. Each of the outer pairs is at a distance a from that in the centre.

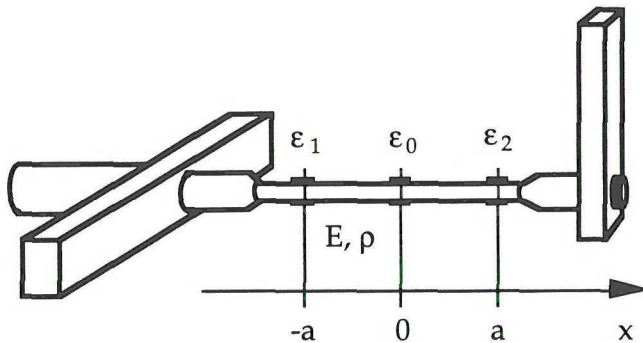


Figure 1. Instrumented linearly viscoelastic member of a structure.

Longitudinal as well as other types of waves are generated in the uniform instrumented part of the member as a result of impact loading of the structure. Let $\epsilon(x,t)$ be the axial strain associated with these longitudinal waves at the cross-section x and the time t . Then the one-dimensional equation of axial motion can be expressed

$$\partial^2 \hat{\varepsilon} / \partial x^2 - \gamma^2 \hat{\varepsilon} = 0, \quad (1)$$

where $\hat{\varepsilon}(x, \omega)$ denotes the Fourier transform of $\varepsilon(x, t)$, and where

$$\gamma^2 = -\rho \omega^2 / E. \quad (2)$$

The wave propagation coefficient can be expressed $\gamma(\omega) = \alpha(\omega) + ik(\omega)$ where $\alpha(\omega)$ is the damping coefficient and $k(\omega)$ is the wavenumber. The real and imaginary parts of E are related to those of γ through

$$E' = \rho \omega^2 (k^2 - \alpha^2) / (k^2 + \alpha^2)^2, \quad E'' = \rho \omega^2 (2k\alpha) / (k^2 + \alpha^2)^2, \quad (3)$$

respectively.

The general solution of equation (1) is

$$\hat{\varepsilon}(x, \omega) = \hat{P}(\omega) e^{-\gamma(\omega)x} + \hat{N}(\omega) e^{\gamma(\omega)x} \quad (4)$$

where $\hat{P}(\omega)$ and $\hat{N}(\omega)$ are functions determined by boundary and initial conditions. In particular, the Fourier transforms of the strains at the three instrumented cross-sections $x = 0$, $x = -a$ and $x = a$ are

$$\hat{\varepsilon}_0(\omega) = \hat{\varepsilon}(0, \omega), \quad \hat{\varepsilon}_1(\omega) = \hat{\varepsilon}(-a, \omega), \quad \hat{\varepsilon}_2(\omega) = \hat{\varepsilon}(a, \omega), \quad (5)$$

respectively. Substitution of equation (4) into equations (5) provides three relations from which the three unknown functions $\hat{P}(\omega)$, $\hat{N}(\omega)$ and $\gamma(\omega)$ can be determined. For the wave propagation coefficient γ there is the result

$$\cosh(\gamma a) = \Psi \quad (6)$$

where

$$\Psi = (1/2)(\hat{\varepsilon}_1 + \hat{\varepsilon}_2) / \hat{\varepsilon}_0. \quad (7)$$

The same relation for γ is obtained if any other displacement-related quantity, i.e. acceleration, is chosen instead of strain.

A geometrical illustration of the relation between the complex quantities $\hat{\epsilon}_1/\hat{\epsilon}_0$, $\hat{\epsilon}_2/\hat{\epsilon}_0$ and $\Psi = re^{i\phi}$ is given in Figure 2. According to equation (6) the quantity Ψ depends on the material through the wave propagation coefficient γ and on the geometry through the distance a , but it is independent of the excitation of the structure. In contrast, the strain ratios $\hat{\epsilon}_1/\hat{\epsilon}_0$ and $\hat{\epsilon}_2/\hat{\epsilon}_0$ do depend on the excitation.

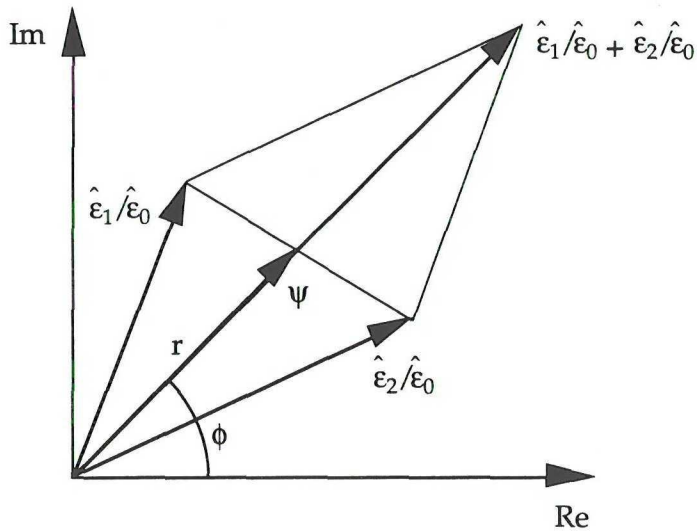


Figure 2. Geometrical representation of the relation between the complex quantities $\hat{\epsilon}_1/\hat{\epsilon}_0$, $\hat{\epsilon}_2/\hat{\epsilon}_0$ and $\Psi = re^{i\phi}$.

From equation (6) the wave propagation coefficient $\gamma = \alpha + ik$ can be expressed in terms of the magnitude r and the phase ϕ of Ψ by substituting r for $r/2$ in the solution obtained by Lundberg and Blanc [5] for a related problem. The result is

$$\alpha = (1/a)\sinh^{-1}[(C-A)^{1/2}], \quad k = (1/a)(s\beta + n\pi), \quad (8)$$

where

$$C = (A^2 + B^2)^{1/2}, \quad A = (1/2)(1-r^2), \quad B = r\sin(\phi), \quad (9)$$

$$\beta = \sin^{-1}[(C+A)^{1/2}].$$

The integers $s = \pm 1$, and $n = 0, 1, 2, \dots$ are chosen according to Table 1, so that $k(\omega)$ is a continuous and monotonically increasing function with $k(0) = 0$. Once α and k have been determined, the real part E' and the imaginary part E'' of the complex modulus E can be obtained from relations (3).

Table 1. Wavelength λ , phase ϕ , parameter β and integers s and n versus radian frequency ω .

ω	0	\uparrow	\uparrow	\uparrow	\uparrow	\uparrow	\uparrow	\uparrow
$\lambda/4$	∞	\downarrow	a	\downarrow	$a/2$	\downarrow	$a/3$	\downarrow
$\sin(\phi)$	0		0		0		0	
$\cos(\phi)$		0		0		0		
β	0	\uparrow	$\pi/2$	\downarrow	0	\uparrow	$\pi/2$	\downarrow
s	1	-1	1	-1	1	-1	1	
n	0		1		2		3	

3. EXPERIMENTAL DEMONSTRATION

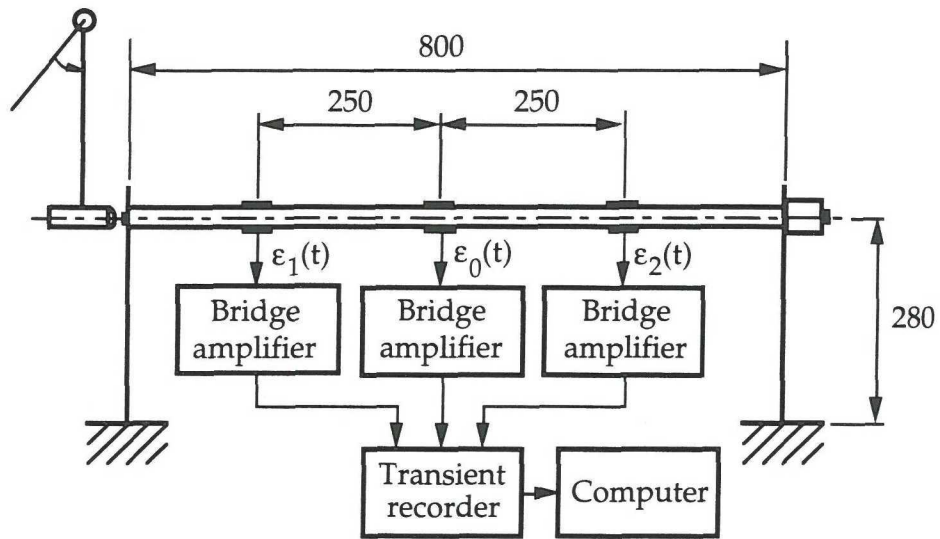
In-situ tests were performed on two simple frame-structures as illustrated in Figure 3. The first structure (I) consisted of a polypropylene bar member and two steel cantilever beam members. The second structure (II) was obtained from the first by attaching a steel lump member at the right end of the polypropylene bar. Both structures were impacted by a pendulum hammer at the left end of the polypropylene bar, in the direction of the bar axis.

The polypropylene bar had length 800 mm, diameter 16 mm and density 919 kg/m³. The cantilever beams had length 280 mm, width 30 mm and thickness 1 mm. The hammer had length 30 mm and diameter 15 mm, and the length of the pendulum was 200 mm. The swing angle was 10 ° as in [6], and the temperature during the tests was 21 °C.

Three pairs of semiconductor strain gauges (Kyowa KSP-2-E4) were attached to the polypropylene bar. In each pair the gauges were diametrically opposite to each other and connected to a Wheatstone bridge in such a way that contributions from bending were eliminated. The signals representing the strains ε_0 , ε_1 and ε_2 were amplified by bridge amplifiers (Measurement Group System 2200), recorded by a transient recorder (Datalog 6034) and transferred to a computer (HP 9100). The quantity $\Psi = (1/2)(\hat{\varepsilon}_1 + \hat{\varepsilon}_2)/\hat{\varepsilon}_0$ was computed from ten tests as the ratio of the average cross-spectrum between $(1/2)(\varepsilon_1 + \varepsilon_2)$ and ε_0 to the average auto-spectrum of ε_0 .

Tests were also made on the dismounted polypropylene bar member using a different method [6] based on measurement of end-point accelerations. The swing angle and the temperature were the same as above. The results for the complex modulus obtained from the *in-situ* tests on the two structures and from the tests on the dismounted member are compared in Figure 4.

(a)



(b)

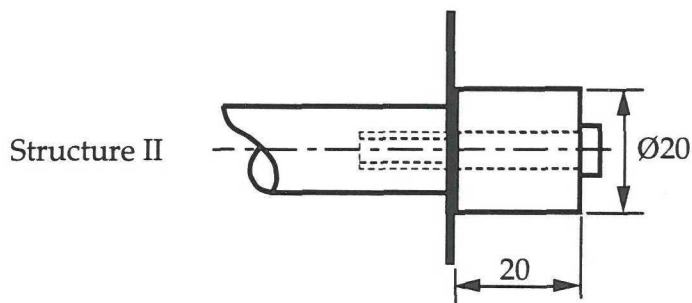
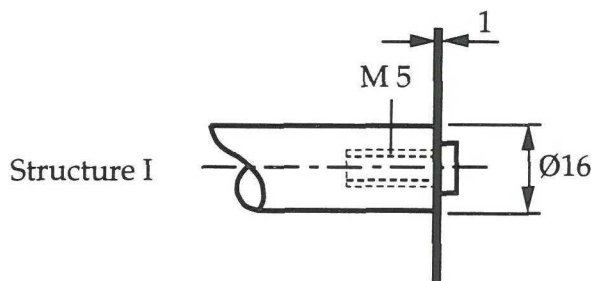


Figure 3. (a) Experimental set-up. (b) Details of structures I and II.

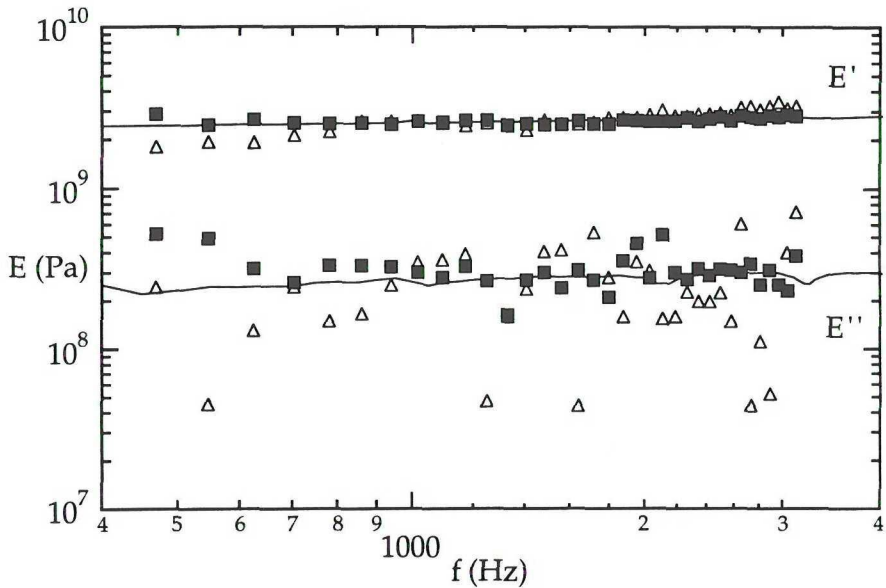


Figure 4. Complex modulus $E = E' + iE''$ versus frequency f obtained from tests on structure I (■), on structure II (Δ), and on the dismounted member of these structures (—).

4. DISCUSSION

A method has been proposed for *in-situ* determination of complex modulus from strains measured at three cross-sections of a member of an impact-loaded structure. The method was demonstrated on a polypropylene bar member of two simple frame structures and results were obtained in the frequency range of approximately 500 Hz to 3 kHz. Corresponding results were obtained for the same member, dismounted from the structures, using a different method based on the measurement of end-point accelerations.

As can be seen in Figure 4 there is a fair agreement between the results from the *in-situ* measurements on the two frame-structures and that from measurements on the dismounted member. It can be observed that there is considerably more scatter in the imaginary parts than in the real parts of the complex modulus. This is a property of the present method as well as related methods [2, 5-7]. Furthermore, there is more scatter in the results obtained with strain gauges in the *in-situ* tests than in that obtained with

accelerometers in the test on the dismounted member, especially for the imaginary part of the complex modulus. A comparison of the results in [5] and [6] also indicates that accelerometers are better suited than strain gauges for this kind of measurements, in the sense that they give less scatter in the results for the complex modulus. However, strain gauges were used for practical reason.

Although the presented theoretical solution is valid for arbitrary boundary conditions, the surrounding structure may influence the scatter but not the average value of the results, as seen in Figure 4. This is due to the effect of the structure on the excitation of the member under consideration and thus on the signal to noise ratio in the measurements.

The present method is expected to have similar properties and limitations as the related methods presented in [2, 5-7]. They can be summarized as follows: (i) More precise results are obtained when the method is used on a material with high internal damping than on one with low internal damping. Results are obtained in a limited frequency interval. (ii) The lower bound of this interval is determined by the distance between the gauges. A larger distance lowers this bound. (iii) The upper bound of the interval is mainly determined by the excitation of the member at hand. To get results in a frequency interval one must, of course, have sufficient excitation in that interval. Furthermore, since one-dimensional theory is used, the transversal dimension of the member at hand must be small compared to the shortest wavelength. In the tests presented here the shortest wavelength, corresponding to 3 kHz, was approximately thirty times the diameter of the bar member. Thus, there should have been no significant three-dimensional effects. The upper bound 3 kHz was determined by the excitation.

As the quantity Ψ is determined from $\varepsilon_1 + \varepsilon_2$ and ε_0 it is noted that it would also be possible to use a standard two-channel spectrum analyzer in combination with an analogue sum circuit. Finally, it is noted that this method can be generalized to cope with structural members without uniform parts by using similar ideas as in [8, 9].

Acknowledgements - The authors are in debt to the Carl Trygger Research Foundation and to the Swedish Institute for their support.

REFERENCES

1. D. M. NORRIS JR and W. C. YOUNG, Complex modulus measurement by longitudinal vibration testing. *Experimental Mechanics* **10**, 93-96 (1970).
2. T. PRITZ, Transfer function method for investigating the complex modulus of acoustical materials: Rod-like specimen. *Journal of Sound and Vibration* **81**, 359-376 (1982).
3. T. BEDA, *Modules complexes des matériaux viscoélastiques par essais dynamiques sur tiges. Petites et grandes déformations. Modélisation, instrumentation, caractérisation*, Doctoral Thesis, Conservatoire National des Arts et Métiers de Paris (1990).
4. R. H. BLANC, *Détermination de l'équation de comportement des corps viscoélastiques linéaires par une méthode d'impulsion* Doctoral Thesis, Université d'Aix-Marseille (1971). Published in part in *Problèmes de la rhéologie* (W. K. Nowacki, editor) 65-85 (1973), IPPT PAN, Warsaw.
5. B. LUNDBERG and R. H. BLANC, Determination of mechanical material properties from the two-point response of an impacted linearly viscoelastic rod specimen. *Journal of Sound and Vibration* **126**, 97-108 (1988).
6. S. ÖDEEN and B. LUNDBERG, Determination of complex modulus from measured end-point accelerations of an impacted rod specimen. *Journal of Sound and Vibration* **163**, (1993). To appear.
7. J. L. BUCHANAN, Numerical solution for the dynamic moduli of a viscoelastic bar. *The Journal of the Acoustical Society of America* **81**, 1775-1786 (1987).
8. B. LUNDBERG, J. CARLSSON and K. G. SUNDIN, Analysis of elastic waves in non-uniform rods from two-point strain measurement. *Journal of Sound and Vibration* **137**, 483-493 (1990).
9. B. LUNDBERG, Characterization of elastic and viscoelastic waves, materials and structures from measurements on a dynamically loaded rod. *Mécanique, modélisation numérique et dynamique des matériaux*, 367 - 377. Publications du L.M.A. No 124 (1991), CNRS, Marseille.

C

EFFECTS OF LOAD AND RECOVERY TIME ON THE COMPLEX MODULUS OF POLYOXIMETHYLENE

S. ÖDEEN * AND R. H. BLANC **

* Department of Mechanical Engineering, Luleå University of Technology
S-951 87 Luleå, Sweden

** Laboratoire de Mécanique et d'Acoustique, CNRS
31, Chemin Joseph-Aiguier, F-13402 Marseille Cedex 20, France

Abstract - The complex modulus of polyoximethylene has been determined during recovery from creep loads of various stress levels and load durations. The determination was performed using a method based on measured end-point accelerations of an impacted rod specimen. The loss factor was found to be considerably higher and the absolute value of the complex modulus slightly lower during recovery compared to the corresponding values for the virgin specimens. The complex modulus recovered completely its initial value within approximately five hours. A simple nonlinear rheological model was employed to describe the time-dependent behaviour of the loss factor.

1. INTRODUCTION

Measuring the complex modulus, in particular the mechanical loss factor, is one of the basic ways of studying and characterizing polymeric materials. Several papers have been published on the transient behaviour of the loss factor during creep [1-5] and relaxation processes [3] in various polymeric materials. In [1, 2] the influence of the thermal history on this behaviour was studied. It was observed that the behaviour of the loss factor during creep and relaxation processes is closely related to those processes themselves. In these investigations the loss factor was studied by superimposing small harmonic perturbations on large static deformations. Reversible changes in the complex modulus have also been observed during periodic loads of polymers, e.g. [7], and during plastic deformation of metals, e.g. [8].

It has been suggested that the observed behaviour could be accounted for by means of nonlinear viscoelastic models. Several models of this kind have been proposed, for example in the case of glassy polycarbonate by Othmezouri-Decerf [1, 2] and in the case of polyethylene by Kubát et. al. [3, 6].

The measurements cited above were carried out at relatively low frequencies between 0.1 and 10 Hz. Ödeen and Lundberg [9] developed a method for determining the complex modulus at frequencies of up to 20 kHz. The complex modulus is obtained from the response of a rod specimen that is subjected to a slight axial impact. The superimposed perturbation is small and the measurement time is short. The former property is important when making measurements on nonlinear materials, while the latter is important when the complex modulus changes rapidly. In the present study this method was employed to investigate the behaviour of the complex modulus of polyoximethylene during creep recovery. Various creep loads were applied in order to examine the influence of stress level and load duration. Furthermore, the complex modulus was measured during recovery from a periodic load superimposed on a static load. Finally, A simple nonlinear rheological model was used to describe the behaviour during creep recovery.

2. EXPERIMENTS

Tests were performed on polyoximethylene. Rod specimens measuring $12 \times 13 \times 500$ mm were cut from plates 13 mm thick. The density of the material was 1400 kg/m^3 .

The complex modulus $E^* = E e^{i\delta}$ was determined at frequency 10 kHz using the method developed by Ödeen and Lundberg [9]. Accelerometers were attached to the ends of the specimen and one end was given a slight axial impact by means of a pendulum steel hammer. The complex modulus of the material was then determined from the measured end-point accelerations. The frequency 10 kHz was chosen in order to, with the chosen geometry of the specimens, give a maximal precision in the determination. The maximum axial stress caused by the impact was approximately 0.3 MPa. The experimental set-up is described in detail in [9].

Creep loads as well as periodic axial loads were applied to the specimens with a hydraulic Instron 1272 testing machine. The tests with creep loads were performed in the following manner: The complex modulus E_0^* was determined for the virgin specimen. A constant axial tensile stress σ_a was applied during a time t_a . During the recovery from that load the complex modulus was determined repeatedly. Five tests (Test 1-5) were conducted with three different stress levels σ_a and three different load durations t_a , see Table 1. All tests with

creep loads were carried out at ambient temperature (23-26 °C). During each test the temperature fluctuation was less than 1 °C.

In the test with periodic load (Test 6) the complex modulus was determined in the virgin specimen in an oven at 31 °C. The specimen was then chilled to room temperature 24 °C. A periodic axial tensile load giving a stress $\sigma(t) = \sigma_a + \sigma_c \sin(2\pi f_c t)$ was applied to the specimen, see Table 1. The frequency f_c was 4 Hz. Due to dissipation in the viscoelastic material the specimen was heated to 31 °C during the periodic load. After the periodic load test the specimen was again put into an oven at 31 °C and the complex modulus was determined repeatedly as above.

Table 1. Test conditions

Test	σ_a (MPa)	σ_c (MPa)	t_a (s)
1	45	—	1800
2	32	—	1800
3	19	—	1800
4	32	—	10800
5	32	—	300
6	32	13	1800

3. MODEL

Assume that the loss factor is $\tan\delta = \tan\delta_0 + \Delta\tan\delta$, where $\tan\delta_0$ is the value for the virgin material and $\Delta\tan\delta$ is the time dependent part. A simple rheological model, Figure 1, has been used to describe the time dependent part $\Delta\tan\delta$. The model consists of two linear springs (E_1 and E_2) and a nonlinear dashpot (η). The model is nonlinear but gives, of course, a linear response to an infinitesimal perturbation superimposed in the nonlinear range of deformation. The complex

modulus in the model is defined as the differential (tangential) modulus for small perturbations of stress and strain.

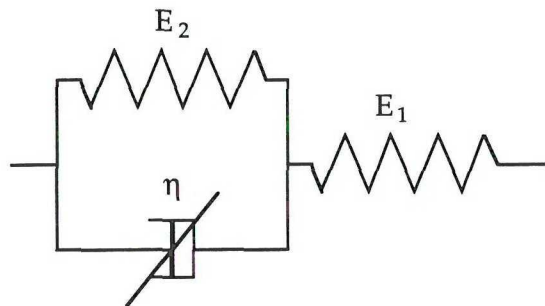


Figure 1. Rheological model consisting of two linear springs (E_1 and E_2) and a nonlinear dashpot (η).

The dashpot is assumed to obey a power-law [10]. The relation between stress σ applied to the dashpot and strain rate $\dot{\epsilon}$ of the dashpot can be expressed

$$\dot{\epsilon} = B \operatorname{sgn}(\sigma) |\sigma|^{m+1} \quad (1)$$

where B and m are constitutive parameters. The differential viscosity η is defined by $\eta = d\sigma/d\dot{\epsilon}$ which gives

$$\eta = 1/\{B(m+1) |\sigma|^m\}. \quad (2)$$

At sufficiently high frequency f , where $E_2 (E_1 + E_2) \ll (\eta 2\pi f)^2$, the time dependent part of the loss factor can be expressed as

$$\Delta \tan \delta = E_1 / (\eta 2\pi f). \quad (3)$$

Consider a material described by this model. The material is subjected to a constant load σ_a at time $t = 0$ and it is unloaded at $t = t_a$ after which the material is free to recover. The loss factor at high frequency as a function of recovery time t is determined from relations (1-3) and from the initial condition that $\dot{\epsilon}=0$ when $t<0$. The result is

$$\Delta \tan\delta = \Delta \tan\delta_i / (t/t_r + 1) \quad (4)$$

where

$$\begin{aligned} \Delta \tan\delta_i &= E_1(m+1)/(E_2 \omega_m t_r), \quad t_r = t_1 / (m[\sigma_a/E_2 - \{mt_a/t_1 + (\sigma_a/E_2)^{-m}\}^{-1/m}]^{-m}), \\ t_1 &= 1/(BE_2^{m+1}). \end{aligned} \quad (5)$$

The model contains four constitutive parameters: E_1 , E_2 , B and m . In the undeformed state the model predicts that $E = E_1$. Therefore E_1 was taken to equal the measured value of E at 10 kHz for the virgin material, i.e., $E_1 = 3100$ MPa. The remaining three parameters were obtained by fitting the results obtained from equations (4) and (5) to the corresponding experimental loss factor data. In equations (4) and (5) it can be seen that for a specific stress level σ_a and load duration t_a there is an infinite number of sets of parameter values which give identical results for $\Delta \tan\delta$. The parameters E_2 , B and m can be determined uniquely only by fitting at least two predicted results with different stress levels σ_a or load durations t_a to the corresponding experimental results. This can be done as follows: The exponent m is specified and E_2 and B are determined, uniquely, from least-square fitting to the result from Test 2. This test was chosen since it gives values of σ_a and t_a which are in the middle of the examined ranges of these load parameters. The procedure is repeated with different m until match is obtained between the predicted results and the results of the other experimental tests. The parameters obtained in this way were $E_2 = 13100$ Pa, $B = 4.55 \cdot 10^{-21}$ Pa \cdot s $^{-2.8}$ and $m = 1.8$.

4. RESULTS

Figures 2 and 3 show the results obtained on the loss factor $\tan\delta$ and the absolute value E of the complex modulus, respectively, at 10 kHz. The results are presented as the time dependent parts $\Delta \tan\delta$ and ΔE as percentages of the values $\tan\delta_0$ and E_0 , respectively, in the virgin material versus recovery time t . Figure 2 shows the results on $\Delta \tan\delta$ obtained in Test 1-5 as well as corresponding theoretical results given by equation 4 and 5. The result on $\Delta \tan\delta$ obtained in Test 6 is also shown here. Figure 3 shows the results on ΔE obtained in Test 1-6.

In the tests at ambient temperature (Tests 1-5) E_0 and $\tan\delta_0$ were approximately 3100 MPa and 0.025, respectively, at 10 kHz. In the test at slightly elevated temperature (Test 6) the corresponding values were 2950 MPa and 0.027.

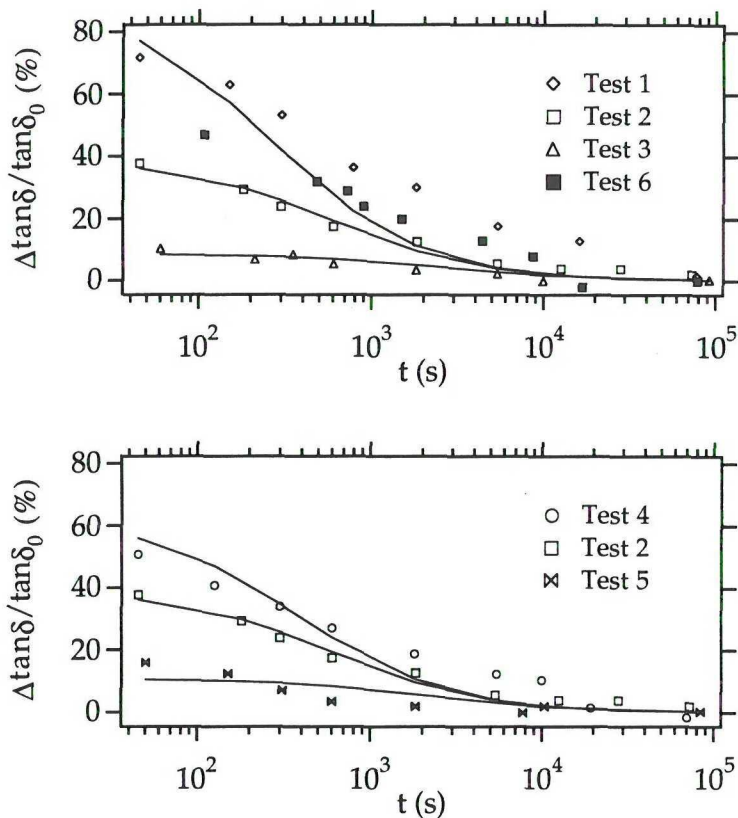


Figure 2. Changes $\Delta\tan\delta$ in the loss factor, as percentages of corresponding value $\tan\delta_0$ in virgin material, versus recovery time t . Open symbols indicate values measured after creep loads. Continuous lines give corresponding theoretical results according to equations 4 and 5. Heavy symbols represent values measured after periodic load.

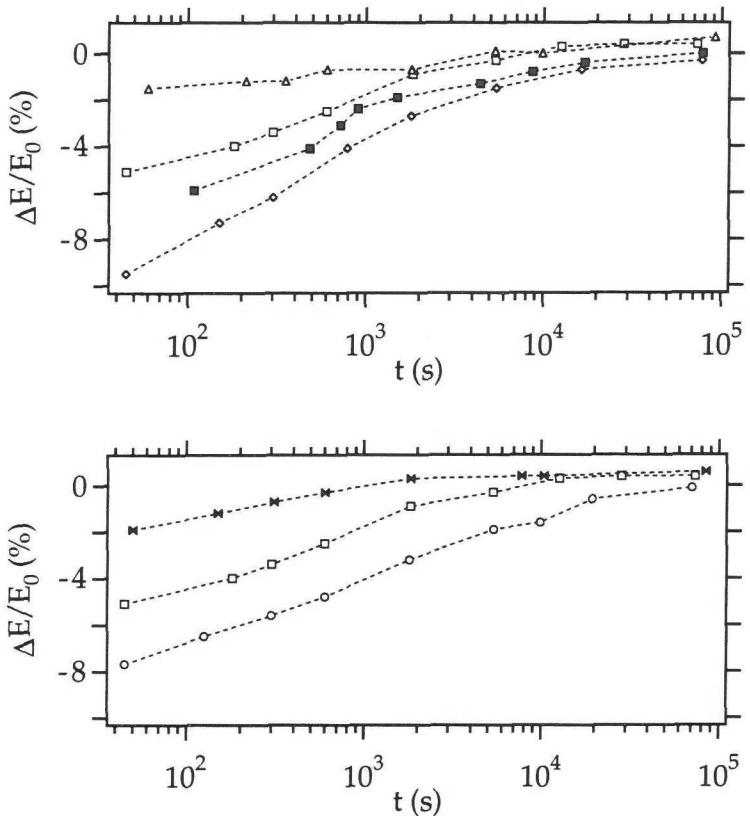


Figure 3. Changes ΔE in the absolute value of the complex modulus, as percentages of corresponding values E_0 in virgin material, versus recovery time t . Symbols as in Figure 2.

5. DISCUSSION AND CONCLUSIONS

The complex modulus has been determined for polyoximethylene during recovery from creep loads of three different stress levels and three different load durations. This was done by superimposing perturbations resulting from slight impacts on the large static deformations. The maximal impact load was approximately 1 % of the applied creep loads. Therefore the perturbation can be considered small. Thus, the determined quantity approximated well the differential complex modulus.

The loss factor $\tan\delta$ was found to be considerably higher than the value obtained on the virgin material and to decrease during the recovery. The absolute value E

of the complex modulus was found on the contrary to be slightly smaller than the value obtained on the virgin material and to increase during the recovery. In all the tests, however, both $\tan\delta$ and E recovered their initial values within approximately five hours from the unloading. The decrease in $\tan\delta$ is in agreement with results published on several polymeric materials [1-5]. The relationship between the magnitudes of the changes $\Delta\tan\delta$ and ΔE and the stress level σ_a is clearly progressive, whereas the relationship between the same magnitudes and the load duration t_a is regressive.

In Test 6 the complex modulus was also determined during recovery from a load with a periodic stress. The maximal value and the average value of that stress were equal to the stress levels in Test 1 and 2, respectively. As was to be expected from the above observed progressive relationship between changes and stress level, the result of Test 6 was in between the results of Tests 1 and 2. It cannot therefore be concluded that the change in the complex modulus in Test 6 was due to fatigue.

A simple nonlinear rheological model was employed to describe the time dependent behaviour of $\tan\delta$ during recovery from creep loads with various stress levels and load durations. As can be seen in Figures 1 and 2, the model gives a qualitatively satisfactory description of the observed behaviour. However, the parameter values used to describe the behaviour of $\tan\delta$ at 10 kHz cannot be used to predict the strain during creep and recovery. This is obvious since a prediction of this kind would give unrealistic values for the strain. The same set of parameter values cannot therefore be used to describe both high frequency properties and slow processes, such as creep and recovery. Furthermore, in [11] it is proposed that the spring E_2 should be a non-Hookean entropy spring if the model is to describe the creep process. In agreement with the experimental results the rheological model predicts a slightly reduced and increasing absolute value E of the complex modulus during recovery. This reduction and increase are much smaller than the measured ones, however. The model is therefore not able to account for the changes in both E and $\tan\delta$. It should be also mentioned that the Eyring-type rheological model proposed in [2] for glassy polycarbonate was also tested. It was found, however, to describe the observed behaviour of polyoximethylene less satisfactory. The above limitations of the model are to be expected from its simplicity. Nevertheless, the results from this investigation indicate that the observed material behaviour can be described by a nonlinear model and that the power-law type of nonlinearity should be chosen.

Acknowledgments - The authors would like to thank Prof. Bengt Lundberg for valuable support and advices. The authors are indebted to the Swedish Institute for its support.

REFERENCES

1. J. Othmezouri-Decerf, *Polymer*, **29** (1988) 641.
2. J. Othmezouri-Decerf, *Polymer Communications*, **32** (1991) 143.
3. J. Kubát, L-Å Nilsson and M. Rigdahl, *Rheologica Acta*, **23** (1984) 40.
4. O. Falk, J. Kubát and M. Rigdahl, *Journal of Materials Science*, **13** (1978) 2328.
5. J. M. Crissman and L. J. Zapas, *Journal of Applied Physics*, **48** (1977) 4049.
6. J. Kubát, M. Rigdahl and R. Seldén, *Journal of Applied Polymer Science*, **20** (1976) 2799.
7. M. Schrager, *Journal of Polymer Science*, **8** (1970) 1999.
8. G. Fantozzi, J. Calvet and P. Gobin, *Journal of the Institute of Metals*, **95** (1967) 169.
9. S. Ödeen and B. Lundberg, Determination of complex modulus from measured end-point accelerations of an impacted rod specimen. *Journal of Sound and Vibration*, **163** (1993). In press.
10. W. N. Findley, J. S. Lai and K. Onaran, *Creep and Relaxation of Nonlinear Viscoelastic Materials*, North-Holland (1976).
11. C. Bauwens-Crowet, J. C. Bauwens, *Journal of Materials Science*, **10** (1975) 1779.

D

IDENTIFICATION OF VISCOELASTIC
MATERIALS FROM ELECTRO-OPTICAL
DISPLACEMENT MEASUREMENTS
AT TWO SECTIONS OF AN
IMPACTED ROD SPECIMEN

I. N. TRENDAFILOVA*, S. ÖDEEN** AND B. LUNDBERG***

*Dept of Mechanics of Deformable Solids, Bulgarian Academy of Sciences, bl. 4, Ac. G.

Bontchev str., 1113 Sofia, Bulgaria

**Dept of Mechanical Engineering, Luleå University of Technology, S-951 87 Luleå, Sweden

***School of Engineering, Uppsala University, Box 534, S-751 21, Sweden

Abstract - A method is proposed for identification of viscoelastic materials from displacements measured at two sections of a cylindrical rod specimen subjected to axial impact. One displacement, considered as excitation, is measured near the impacted end, and another, considered as response, is measured at the free end. Both displacements are measured by means of electro-optical displacement transducers. The first step of the method is model identification, i. e., choice of material model. The second is parameter identification, i. e., determination of the parameters of the model chosen. The problem of model identification is formulated as a pattern recognition one with choice between three Maxwell-type models, one linear and two nonlinear. The problem of parameter identification is solved by minimizing, in the sense of least squares, the difference between simulated and measured velocity responses for the same excitation. The method is applied to five polymers of interest in engineering, viz., polypropylene, polyamide 6, polyoximethylene, high density polyethylene, and 60 percent carbon-black filled natural rubber. The error, expressed as a normalized difference between simulated and measured velocity responses, is approximately 2 percent.

1. INTRODUCTION

In engineering applications there is great need of material models which represent the mechanical properties of real materials with sufficient accuracy. Such models can be chosen, and their parameters can be determined, through identification procedures [1].

Many important engineering materials, such as plastics, rubbers and some metals, exhibit viscoelastic properties under dynamic loads. Therefore, in this paper, we consider identification of such materials under impact

loading conditions. The problem of identification of the complex modulus under such loading conditions has been solved previously by using measurements of strains [2, 3] and end-point accelerations [4] of an impacted rod specimen. Related problems have been solved for yield limits [5] and hardening moduli for structures [6] by applying mathematical programming.

In mechanics identification usually implies *parameter identification*, i. e., determination of the parameters of a material model which has already been chosen [5, 7]. Presently, there is a multitude of models for describing material behaviour. The choice among them, the *model identification*, is usually made intuitively, and is based on the experience and *a priori* knowledge of the investigator. However, this choice can also be made on a mathematical basis [8, 9]. In this paper we choose the latter approach.

The model identification problem is formulated as a pattern recognition one [8, 9] and is solved using a statistical classifier. A general introduction to statistical pattern recognition is given in [10]. The parameter identification problem is solved by minimizing, in the sense of least squares, the discrepancy in response between the model and the real system [11]. Such an approach has been applied also for identification of, e. g., geotechnical system parameters [7]. The solution technique adopted for both the model and the parameter identification problem stems in a stochastic approximation approach introduced by Robbins and Monro [12].

The experimental procedure is based on electro-optical displacement measurements at two sections of an axially impacted rod specimen. Nonlinear as well as linear viscoelastic models of the Maxwell type are considered. First, the identification problem is formulated. Then, the methods for solving the model and parameter identification problems are presented. Finally, the method is applied to five polymeric materials of interest in engineering.

2. METHOD

2.1 Formulation of the problem

Consider a straight, cylindrical, slender and homogeneous rod specimen with density ρ . It is impacted at one end as shown in Figure 1. It is assumed that the longitudinal wave propagation in the specimen is governed by the system of partial differential equations

$$\frac{\partial \sigma}{\partial x} = \rho \frac{\partial v}{\partial t} \quad (1)$$

$$\frac{\partial \epsilon}{\partial t} = \frac{\partial v}{\partial x} \quad (2)$$

$$\Phi\left(\sigma, \epsilon, \frac{\partial \sigma}{\partial t}, \frac{\partial \epsilon}{\partial t}\right) = 0 \quad (3)$$

where $\sigma(x,t)$ is the normal stress, $v(x,t)$ is the particle velocity, and $\epsilon(x,t)$ is the normal strain. Equation (1) is the equation of motion, equation (2) expresses compatibility, and equation (3) is the constitutive relation.

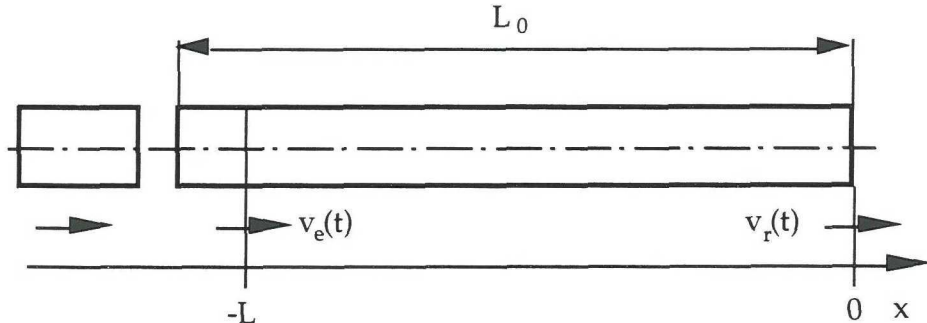


Figure 1. Projectile and rod specimen.

The rod is quiescent at time $t = 0$, i. e., the initial conditions are

$$\sigma(x,0) = 0, \quad v(x,0) = 0. \quad (4)$$

The end $x = 0$ is free and the velocity is considered to be given at $x = -L$, near the impacted end. Therefore the boundary conditions are

$$\sigma(0,t) = 0 \quad (5)$$

and

$$v(-L,t) = v_e(t), \quad (6)$$

where $v_e(t)$ is the given velocity of excitation.

Consider now the class of constitutive relations [13] with

$$\Phi = \frac{1}{E} \frac{\partial \sigma}{\partial t} + F(\sigma) - \frac{\partial \epsilon}{\partial t}. \quad (7)$$

This function represents Maxwell-type models, where $\frac{1}{E} \frac{\partial \sigma}{\partial t}$ is the elastic and $F(\sigma)$ the inelastic part of the strain rate. The quantity E is Young's modulus.

The response in particle velocity $v_r(t)$ at the free end $x = 0$ is given by

$$v_r(t) = v(0,t). \quad (8)$$

The *direct* problem considered is as follows: Given Young's modulus E , the constitutive function $F(\sigma)$ and the excitation velocity $v_e(t)$; determine the response velocity $v_r(t)$ by solving simultaneously equations (1) to (8). There are different suitable ways of solving this problem depending on the constitutive relation (3). In what follows the finite system method [14, 15] will be used. This method was chosen as it permits an easy change of the constitutive function F .

The related *identification* problem considered is as follows: Given the excitation velocity $v_e(t)$ and the response velocity $v_r(t)$; determine the constitutive function $F(\sigma)$ and Young's modulus E . As mentioned, the identification consists of two parts, viz., (i) the model identification where, in this case, the *form* of the constitutive function F , is chosen, and (ii) the parameter identification, where Young's modulus E and the constitutive parameters of F are determined.

2.2 Model identification

The choice of the model may be decisive for the ultimate success or failure of the identification scheme. Here the problem for model identification was formulated as a pattern recognition one and was solved using a statistical classifier. We briefly present the three basic steps of the method.

The first step is the *definition of models*. A group of three viscoelastic models M_i ($i = 1, 2, 3$) of the Maxwell type was chosen to represent the material behaviour. These models, together with their constitutive functions F_i and their parameter vectors p_i , are defined in Table 1.

Table 1. Models considered.

i	Model M_i	Constitutive function F_i	Parameter vector p_i^T
1	Maxwell	σ/η	(E,η)
2	Maxwell-Norton	$ \sigma ^k \operatorname{sgn}(\sigma)/B$	(E,k,B)
3	Maxwell-Gurevitch-Rabinovitch	$\sigma \exp(\sigma /m)/\eta$	(E,m,η)

The second step is the *definition of pattern vectors and standard samples*. A pattern vector y is defined by [9]

$$y^T = (y^1, y^2, \dots, y^n), \quad y^k = |v_e(t_k) - v_r(t_k)|, \quad (9)$$

where the superscript T denotes the transposed vector. Standard samples y_{ij} of these pattern vectors were formed for each experimental test by solving for each model M_i the direct problem with different parameter vectors p_{ij} ($j = 1, 2, \dots, N_i$) and the measured excitation $v_e(t)$. For each model, about sixty parameter vectors were taken from available experimental results for

similar materials, mostly polymers, under similar conditions. For details, see [9].

The third step is the *solution of the pattern recognition problem*. This was done by comparing the pattern vector \mathbf{y} , obtained from an experimental test, with the standard samples \mathbf{y}_{ij} of this vector. A stochastic supervised classifier was used to obtain adequacy measures $P_i(\mathbf{y})$ for representing the material behaviour with the different models M_i . More precisely, the Robbins-Monro stochastic approximation method [16] was applied to evaluate $P_i(\mathbf{y})$. The definition of $P_i(\mathbf{y})$ and the method for obtaining it are presented in detail in [9] (where $P_i(\mathbf{y})$ is referred to as probability for belonging to a class). The adequacy measure $P_i(\mathbf{y})$ has the property $0 \leq P_i(\mathbf{y}) \leq 1$. If $P_i(\mathbf{y}) > P_j(\mathbf{y})$, then the model M_i was considered more adequate than the model M_j . Thus, the model with the highest adequacy measure $P_i(\mathbf{y})$ was chosen.

2.3 Parameter identification

After the choice of constitutive function F_i , the parameter vector \mathbf{p}_i should be determined. The parameter identification was carried out on the basis of similar experimental data as the model identification. The parameter vector \mathbf{p}_i should be determined so that the simulated response velocity $\mathbf{v}_r^s(t)$, obtained by solving the direct problem for the measured excitation velocity $\mathbf{v}_e(t)$, is as close as possible, in some sense, to the measured response velocity $\mathbf{v}_r(t)$.

The measured and simulated response velocity vectors are

$$\mathbf{v}_r^T = \{\mathbf{v}_r(t_1), \mathbf{v}_r(t_2), \dots, \mathbf{v}_r(t_N)\} \quad (10)$$

and

$$\mathbf{v}_r^{s T} = \{\mathbf{v}_r^s(t_1), \mathbf{v}_r^s(t_2), \dots, \mathbf{v}_r^s(t_N)\}, \quad (11)$$

respectively. Suppose that Q different experiments are used, so that the measured and simulated velocity response vectors are \mathbf{v}_{rq} and $\mathbf{v}_{rq}^s(\mathbf{p}_i)$, $q = 1, \dots, Q$, respectively. As there was no information on noise, the most natural method to employ for parameter identification was the least-square one [11].

Therefore the criterion function, which should be minimal for the solution $\mathbf{p}_i = \hat{\mathbf{p}}_i$, was chosen as

$$H(\mathbf{p}_i) = \sum_{q=1}^Q \{\mathbf{v}_{rq} - \mathbf{v}_{rq}^s(\mathbf{p}_i)\}^T \{\mathbf{v}_{rq} - \mathbf{v}_{rq}^s(\mathbf{p}_i)\}. \quad (12)$$

Minimisation with respect to \mathbf{p}_i leads to

$$\frac{\partial H}{\partial \mathbf{p}_i} = 2 \sum_{q=1}^Q \left(\frac{\partial \mathbf{v}_{rq}^s}{\partial \mathbf{p}_i} \right)^T \{\mathbf{v}_{rq}^s - \mathbf{v}_{rq}\} = 0. \quad (13)$$

We used the Robbins-Monro [16] algorithm for stochastic approximation, which gave the iterative procedure

$$\mathbf{p}_i(m+1) = \mathbf{p}_i(m) - \frac{1}{m} \frac{\partial H}{\partial \mathbf{p}_i} \Big|_{\mathbf{p}_i = \mathbf{p}_i(m)} \quad (14)$$

for determining the solution $\hat{\mathbf{p}}_i$. This algorithm has the advantage of being convergent for any initial guess of the parameter vector, provided that H is continuous and that the derivative in equation (14) exists. After three iterations we switched to the Davidon-Power-Fletcher method in order to make the convergence faster. An algorithm for this method is given in [17]. A comparison of a pre-assigned tolerance with the rate of improvement of \mathbf{p}_i was used as a convergence criterion.

Verification of the correctness of the procedure for parameter identification is given in the Appendix.

3. EXPERIMENTS

Experimental tests were carried out at the ambient temperature 20 °C on four commercially available plastics, viz., polypropylene, polyamide 6, polyoximethylene and high density polyethylene. Tests were also carried out on 60 percent carbon-black filled natural rubber. Cylindrical rod specimens with circular cross-sections of diameter D were used. The plastics

were tested with four specimen lengths L_0 , while the rubber was tested with two specimen lengths. Five tests were performed for each material. The test conditions are given in Table 2.

The experimental set-up is shown in Figure 2. The specimen was suspended in bushings made of polyoximethylene with the diameter of the hole slightly larger than that of the specimen. Furthermore, the specimen was impacted axially by an aluminium projectile which was accelerated by a spring-driven gun. The length of the projectile was 30 mm, and its diameter was 15.8 mm. In all tests the impact velocity of the projectile was 10 m/s.

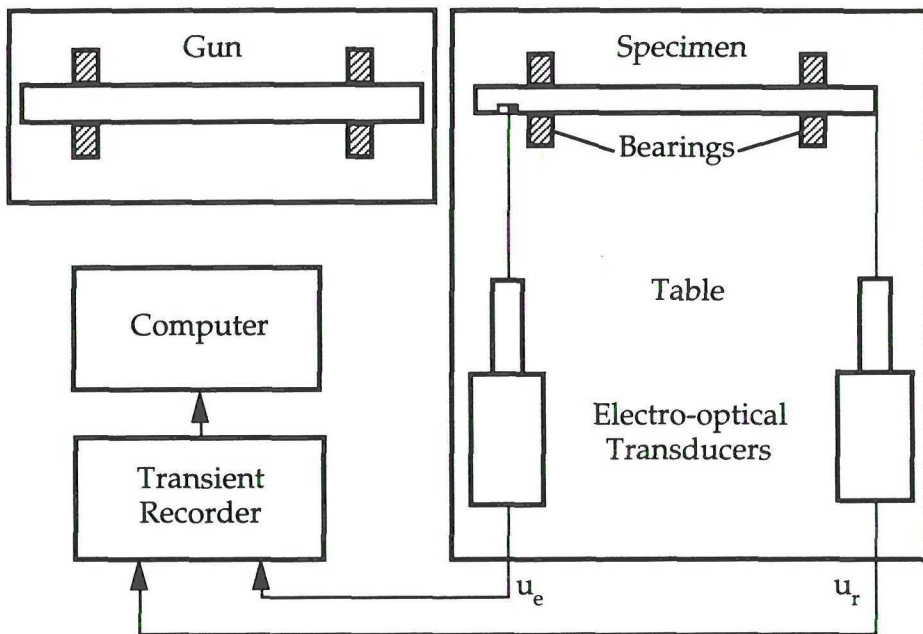


Figure 2. Experimental set-up.

In order to obtain the velocities $v_e(t)$ and $v_r(t)$, the corresponding displacements $u_e(t)$ and $u_r(t)$ were measured and differentiated numerically. Electro-optical displacement transducers (Zimmer 100D) were used. These are devices for contactless measurement of a linear displacement of a contrasting edge. For the response displacement u_r the contrast between the end surface of the specimen and the illuminated background was used, while for excitation displacement u_e the contrast between small pieces of

coloured tape was used. The fact that it would have been difficult to obtain a well-defined contrasting edge at the impacted end was the reason for measuring u_e at an interior section of the specimen rather than at the impacted end. In each test the lenses of the transducers were chosen in order to obtain a suitable range of measurement. In Tests 1-5 the range was 5 mm, while it was 20 mm in the other tests.

Table 2. Test conditions

Test	Material	ρ (kg/m ³)	D (mm)	L_0 (mm)	L (mm)
1	Polypropylene	910	15.7	400	394
2		910	15.5	200	190
3		910	15.5	400	392
4		910	15.5	600	593
5		910	15.5	788	781
6	Polyamide 6	1140	15.6	400	391
7		1140	16.6	201	193
8		1140	16.6	400	392
9		1140	16.6	600	590
10		1140	16.6	800	791
11	Polyoximethylene	1400	15.5	400	388
12		1400	15.5	200	192
13		1400	15.5	400	388
14		1400	15.5	600	590
15		1400	15.5	800	790
16	Polyethylene	940	16.1	400	378
17		940	16.1	200	193
18		940	16.1	400	378
19		940	16.1	600	586
20		940	16.1	800	784
21	Rubber	1320	12.2	402	392
22		1320	12.2	199	195
23		1320	12.2	199	195
24		1320	12.2	402	392
25		1320	12.2	402	392

The signals from the transducers were fed to a transient recorder (Tektronix 2630). The sampling frequency was 51.2 kHz. The analysis of the signals was carried out on a PC (Compaq Deskpro 386s).

In order to avoid disturbances of the measurements from the recoil of the gun, the specimen and the transducers were mounted on a table separate from the one on which the gun was mounted.

4. RESULTS

The results of model identification based on the first test for each material, following the order in Table 2, are presented in Table 3, which gives the adequacy measure P_i associated with each of the three models for each material. The model with bold face adequacy measure was chosen for each material.

Table 3. Adequacy measure P_i . Maximum adequacy measure bold face for each material.

Material	Adequacy measure		
	P_1	P_2	P_3
Polypropylene	0.220	0.712	0.106
Polyamide 6	0.705	0.623	0.430
Polyoximethylene	0.299	0.600	0.569
Polyethylene	0.727	0.231	0.785
Rubber	0.012	0.655	0.842

The data from the remaining four tests for each material were used to identify the parameter vectors of the models chosen. Four parameter vectors \hat{p}_i^Q were determined for each material, where $Q = 1, 2, 3, 4$ indicates that the tests $q=1,\dots,Q$ were used. For each material $q = 1, 2, 3, 4$ corresponds

to the 2nd, 3rd, 4th, 5th test, respectively. The elements of the parameter vectors $\hat{\mathbf{p}}_i^4$ for the investigated materials are given in Table 4.

Table 4. Result of model and parameter identification.

Material	Model	Parameters
Polypropylene	M_2	$E = 2.580 \text{ GPa}$ $\kappa = 2.108$ $B = 38.16 \text{ EPa}^\kappa s$
Polyamide 6	M_1	$E = 3.209 \text{ GPa}$ $\eta = 40.85 \text{ GPas}$
Polyoximethylene	M_2	$E = 2.911 \text{ GPa}$ $\kappa = 1.876$ $B = 7.917 \text{ EPa}^\kappa s$
Polyethylene	M_3	$E = 2.107 \text{ GPa}$ $\eta = 314.6 \text{ GPas}$ $m = 7.082 \text{ TPa}$
Rubber	M_3	$E = 276.6 \text{ MPa}$ $\eta = 81.20 \text{ GPas}$ $m = 108.9 \text{ GPa}$

For the model M_i and the number of tests Q the error

$$\delta_i^Q = \frac{1}{V_0} \left\{ \frac{1}{N_Q} H(\hat{\mathbf{p}}_i^Q) \right\}^{1/2}$$

was calculated. Here N_Q is the total number of elements in the vectors \mathbf{v}_{r1} , \mathbf{v}_{r2} , ..., \mathbf{v}_{rQ} . The characteristic velocity V_0 was taken to be the impact velocity. The errors are given in Table 5.

Table 5. Average error $\bar{\delta}_i^Q$ in percent.

Material	Model	Error in percent			
		$\bar{\delta}_i^1$	$\bar{\delta}_i^2$	$\bar{\delta}_i^3$	$\bar{\delta}_i^4$
Polypropylene	M_2	1.90	1.78	1.76	1.75
Polyamide 6	M_1	1.60	1.98	2.10	2.15
Polyoximethylene	M_2	2.08	2.06	1.89	1.77
Polyethylene	M_3	1.98	2.10	1.75	2.06
Rubber	M_3	1.76	1.75	1.91	1.93

5. DISCUSSION

A method has been proposed for identification of viscoelastic materials from electro-optical displacement measurements at two sections of an impacted rod-specimen. Model as well as parameter identification have been considered.

The errors δ_i^Q given in Table 5 are measures of the agreement obtained between the measured and the simulated responses using the different models. It can be seen in Table 5 that, for all materials tested, the errors δ_i^Q remain approximately constant, at a level around 2 percent, when Q is increased, i. e., when new tests with different specimen geometries are included in the parameter identification procedure. This confirms that the model chosen for each material in the model identification is suitable for representing the behaviour of the material under load conditions similar to those in the experiments.

Here, the model with the highest adequacy measure P_i was chosen to represent the material behaviour. For several of the tested materials,

however, two different models have high values of P_i which are relatively close. In such cases one might also choose the simplest of these two models. For the polyethylene, for instance, one might prefer the linear model M_1 instead of the nonlinear model M_3 for the sake of simplicity.

Due to the use of contactless electro-optical transducers, the experimental procedure involves a very simple specimen preparation, and also in other respects the procedure is convenient and fast. Therefore the method is meant to be suitable for quick routine testing of viscoelastic materials.

Acknowledgements - The authors are indebted to the Carl Trygger Research Foundation, the Research Council of Norrbotten and the Swedish Academy of Engineering Sciences for their support.

REFERENCES

1. L.A. ZADEH, From circuit theory to system theory. *Proc IRE*, **50**, 856-865 (1962).
2. B. LUNDBERG and R.H. BLANC, Determination of mechanical material properties from the two-point response of an impacted linearly viscoelastic rod specimen. *Journal of Sound and Vibration* **126**, 97-108 (1993).
3. B. LUNDBERG and S. ÖDEEN, In-situ determination of complex modulus from strain measurements on an impacted structure. *Journal of Sound and Vibration*. **166**, (1993) In press.
4. S. ÖDEEN and B. LUNDBERG, Determination of complex modulus from measured end-point accelerations of an impacted rod specimen. *Journal of Sound and Vibration*, **163**, (1993) In press.
5. G. MAIER, F. GIANESSI and A. NAPPI, Indirect identification of yield limits by mathematical programming. *Eng. Struct.* **4**, 86-98 (1982).
6. A. NAPPI, System identification for yield limits and hardening moduli in discrete elastic-plastic structures by nonlinear programming. *Appl. Math. Modelling*, **6**, 441-448, (1982).

7. A. GIVIDINI, G. MAIER and A. NAPPI, Parameter estimation of a static geotechnical model using a Bayes approach. *Int.J. of Rock Mech. Min. Sci. Geomech. Abstr.* **20**(5), 215-226 (1983).
8. I. NICOLLOVA-TRENDAFILOVA, On the problem of mechanical systems constitutive modelling using the theory of pattern recognition. *Systems, Analysis, Simulation* **1**, 71-74 (1990).
9. I. TRENDAFILOVA, On a method for mechanical-mathematical model identification using a stochastic pattern recognition approach. *European Journal of Mechanics A-Solids* **11**, 767-779 (1992).
10. K. FUKUNAGA, *Introduction to statistical pattern recognition*, Acad.Press, (1972).
11. P. EYKHOFF, *System identification*. J.Wiley & Sons (1974).
12. H. ROBBINS and S. MONRO, A stochastic approximation method. *Ann. Math. Stat.* **22**, 400-407, (1951).
13. R.M. CHRISTENSEN, *Theory of viscoelasticity. An introduction*, Second ed., Acad. Press (1982).
14. A.R. MITCHELL and D.F. GRIFFITHS, *The finite difference method in partial differential equations*, J.Wiley & Sons (1980).
15. A. BALTOV, Application of mathematical system theory to dynamical thermoplasticity, *ZAMM* **58**, T195-T197 (1978).
16. J. TOU and R. GONZALEZ, *Pattern recognition principles*. Addison-Wesley Publ.Comp. (1974).
17. M.A. WOLFE, *Numerical methods for unconstrained optimization, an introduction*, Van Nostrand Reinhold C. (1978).

APPENDIX

In order to verify the correctness of the procedure for parameter identification, some numerical tests were carried out with simulated experiments. Thus, the output of the direct problem was used as input of the identification problem, and it was checked to which extent the output parameter vector of the latter agreed with the input parameter vector of the former.

The rod specimens were assumed to have the distance between transducers $L = 400$ mm and the diameter $D = 16$ mm. The densities ρ of the specimens and the results are given in Table A1. The discrepancies between the output and input parameters are between 0.06 percent and 1.3 percent, which is considered to be satisfactory.

Table A1. Input and output parameter vectors p_i .

Model	ρ (kg/m ³)	p_i (input)	p_i (output)	Relative error (%)
M ₁	1100	$E = 3.056$ GPa $\eta = 11.12$ GPas	$E = 3.060$ GPa $\eta = 10.98$ GPas	0.13 1.3
M ₂	1400	$E = 2.500$ GPa $\kappa = 1.550$ $B = 320.0$ TPa κ s	$E = 2.512$ GPa 1.558 319.8 TPa κ s	0.48 0.52 0.06
M ₃	1120	$E = 270.0$ MPa $\eta = 1.110$ GPas $m = 120.0$ GPa	$E = 270.4$ MPa $\eta = 1.108$ GPas $m = 119.7$ GPa	0.15 0.18 0.25

E

PREDICTION OF IMPACT FORCE BY IMPULSE RESPONSE METHOD

S. ÖDEEN AND B. LUNDBERG

Department of Mechanical Engineering, Luleå University of Technology
S-951 87 Luleå, Sweden

Abstract - A method has been established which permits prediction of impact force history from the velocity response of each impacting body to an impulsive force applied to its impact face, and the impact velocity. The bodies may consist of one or several linearly elastic or viscoelastic materials. However, the method is limited to cases of impact without significant effects of friction and slip, with constant contact area and with small deformations. It has been applied to four cases of axial impact of a truncated cone or a compound cylinder on a long cylindrical rod. The truncated cone was made of Nylon-6, the compound cylinder of Nylon-6 and aluminium, and the long cylindrical rod of steel. For the truncated cone and the compound cylinder measured as well as theoretically predicted impulse responses were used, while for the long cylindrical rod only a theoretically predicted impulse response was employed. In all cases good agreement was obtained between the impact force histories predicted, using the impulse response method, and those measured with the aid of strain gauges on the long cylindrical rod. Because of three-dimensional effects the best agreement was obtained for the predictions based on measured impulse responses for the truncated cone and the compound cylinder.

NOTATION

Parameters and variables

A	cross-sectional area
a, b	parameters
C, D	arbitrary functions of w
E	complex modulus
F	impact force
F_i	force acting on impact face of body "i"
F_s	force on impact faces when these stick to each other
G_i	impulse response of body "i"
\hat{G}_i	Fourier transform of G_i
H	Heaviside's unit step function
h	drop height

k	wave number (imaginary part of g)
L	length of section of compound cylinder
m, n	functions of ϕ
P	transition matrix
q	damping coefficient
R	real part of Z
t	time
t_0	duration of impact
t_{tr}	transit time
V	impact velocity
v_i	normal velocity of impact face of body "i"
X	imaginary part of Z
x	axial coordinate
Z	characteristic impedance
α	damping coefficient (real part of γ)
γ	propagation coefficient
ε	axial strain
θ	swing angle
ρ	density
ϕ	ratio of characteristic impedances
ω	angular frequency

Abbreviations

CC	compound cylinder
CCA	compound cylinder with impact face A
CCB	compound cylinder with impact face B
LCR	long cylindrical rod
TC	truncated cone
TCA	truncated cone with impact face A
TCB	truncated cone with impact face B

1. INTRODUCTION

The efficiencies of technological processes such as, for example, percussive drilling [1] depend greatly on the history of generated impact forces. Therefore, there is much interest in either (i) *measuring* or (ii) *predicting* such histories. In the first case, the determination of impact force history demands data which can be obtained only during impact. In the second case such data are not needed.

Measurement of impact force commonly relies on data obtained from a transducer placed between the impacting bodies [2-5]. Such a transducer may, by its presence, influence the impact history. This disadvantage can sometimes be avoided by instead attaching strain gauges or accelerometers to one of the impacting bodies at some distance from the impact face [6-11]. In this case the impact force is determined from the data obtained during impact and a known response of the instrumented body which may have been either predicted, for example [6-8], or measured, for example [9, 11].

Prediction of impact force is generally based on data for the materials and geometries of the impacting bodies, and the impact velocity, in conjunction with an impact model. Thus, the impacting bodies are characterized in a general way, which is suitable also for other problems than the impact problem at hand. As a result, considerable efforts must generally be spent on the mathematical or numerical analyses required for the prediction of impact force history.

This paper deals with a method for prediction of impact force history from the velocity response of each body to an impulsive force applied to its impact face, and the impact velocity. The impulse responses of the impacting bodies can be either measured or predicted. Thus, the impacting bodies are characterized in a way, which is specific to the impact problem at hand. As a result, quite limited mathematical or numerical efforts are needed for the prediction of impact force history. Furthermore, it will be seen that the analyses have the same character independently of the combination of impacting bodies. The method is referred to as the impulse response method.

First, the basic idea of the impulse response method will be presented. Then the method will be applied to four cases of impact of a truncated cone, made of Nylon-6, and a compound cylinder, made of Nylon-6 and aluminium, on a long cylindrical rod made of steel. Both measured and predicted impulse

responses will be used, and comparisons will be made between predicted and measured impact force histories.

2. THE IMPULSE RESPONSE METHOD

Consider impact between two linearly elastic or viscoelastic bodies as illustrated in Figure 1. It is assumed that the impact interface can be attributed a single velocity, and that this velocity and the impact force F are both parallel to the impact velocity V . Furthermore, it is presumed that there are no significant effects of friction and slip, that the contact area is constant and that the deformations are small. Thus, there should be no significant nonlinear effects. The impact force history $F(t)$ is to be determined.

The impacting bodies are characterized by their impulse responses $G_1(t)$ and $G_2(t)$ defined by the convolutions

$$v_1(t) = G_1(t) * F_1(t), \quad v_2(t) = G_2(t) * F_2(t) \quad (1)$$

where $F_i(t)$ is a compressive force acting on the impact face of body "i", and $v_i(t)$ is the corresponding velocity of the same impact face. Before contact is established at time $t = 0$, the first body has the impact velocity V and the second is at rest.

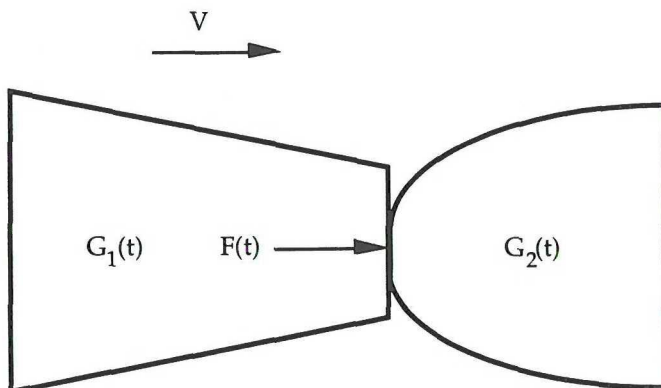


Figure 1. Impact between bodies with impulse responses $G_1(t)$ and $G_2(t)$. The impact velocity is V and the impact force $F(t)$.

Provisionally it is assumed that the two impact faces stick to each other when they come in contact, and that they interact with a force $F_s(t)$ which is positive in compression. For $t \geq 0$ the velocity of the first impact face is $V - G_1 * F_s$, while that of the second is $G_2 * F_s$. As these velocities must be the same, the force $F_s(t)$ satisfies the integral equation [12]

$$[G_1(t) + G_2(t)] * F_s(t) = VH(t) \quad (2)$$

where $H(t)$ is Heaviside's unit step function.

From the nature of the problem it is clear that the force $F_s(t)$ is initially compressive, that is, positive. If (i) it remains non-negative for all $t > 0$ it is equal to the impact force $F(t)$ of the original problem, and the duration of impact is infinite. If (ii) it ceases to be non-negative at $t = t_0$ the impact force of the original problem is

$$F(t) = F_s(t) [H(t) - H(t - t_0)] \quad (3)$$

and the duration of impact is t_0 . This relation is generally valid if t_0 is considered to be infinite in the first case.

According to the impulse response method the impact force is predicted using Equations (1) to (3). This can be done, using different analytical and numerical techniques, in the time domain or in the frequency domain, where the convolutions in Equations (1) and (2) turn into multiplications. In this paper use has been made of Fourier transforms, discrete Fourier transforms, and the fast Fourier transform algorithm.

3. IMPULSE RESPONSE

3.1. Measurement

The axial impulse response G_1 was measured at each end, A and B, of the truncated cone (TC) and the compound cylinder (CC) shown in Figure 2. Where convenient, these four cases will be referred to as TCA, TCB, CCA and CCB.

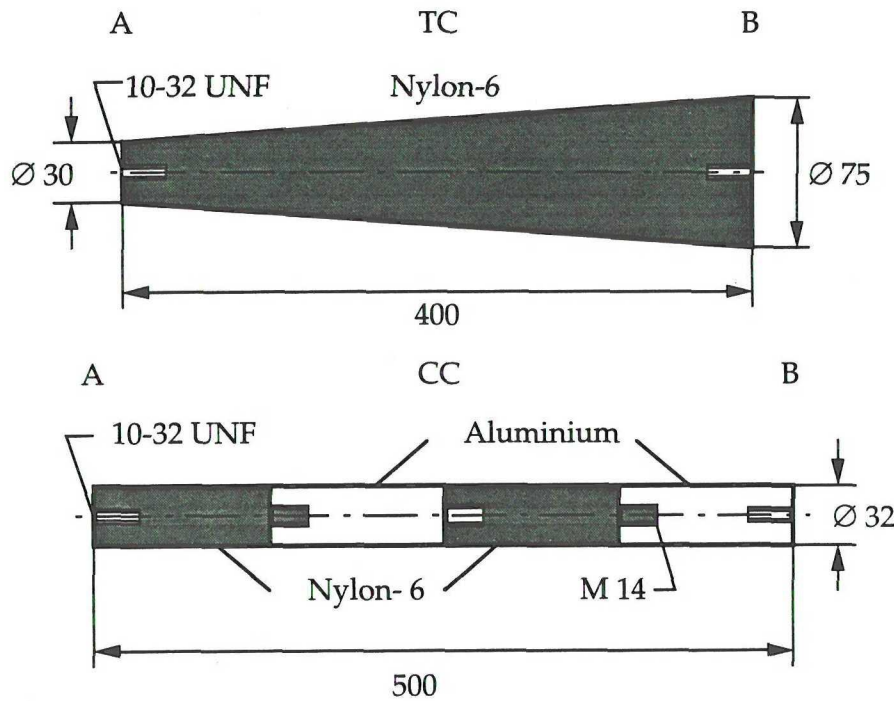


Figure 2. Truncated cone (TC) and compound cylinder (CC) with impact faces A and B.

The truncated cone was made of Nylon-6 and had length 400 mm, and diameters 30 mm at the end A and 75 mm at the end B. The compound cylinder was made of four alternating cylindrical sections of Nylon-6 and aluminium. There was a Nylon-6 section at the end A and an aluminium section at the end B. All sections had length 125 mm and diameter 32 mm, and they were screwed together as shown. At each end of the truncated cone and the compound cylinder there was a threaded hole for attachment of an impedance head.

With this choice of geometries, predictions based on one-dimensional analyses are meaningful although some three-dimensional effects are present. The choice of materials was dictated mainly by the availability of material data.

The experimental set-up is shown in Figure 3 for the case of the truncated cone with impact face A. The body to be tested was suspended in thin cords and it was struck axially by a pendulum steel hammer. The length of the

pendulum was 300 mm. In order to achieve sufficient excitation at all frequencies of interest one light hammer, with length 30 mm and diameter 15 mm, and one heavy hammer, with length 75 mm and diameter 20 mm, were used. The swing angle θ of the pendulum varied in the test cases TCA, TCB, CCA and CCB as follows: For the heavy hammer it was 4.0, 4.0, 4.0 and 3.5°, respectively. For the light hammer it was 6.0, 6.0, 4.0 and 4.0°, respectively.

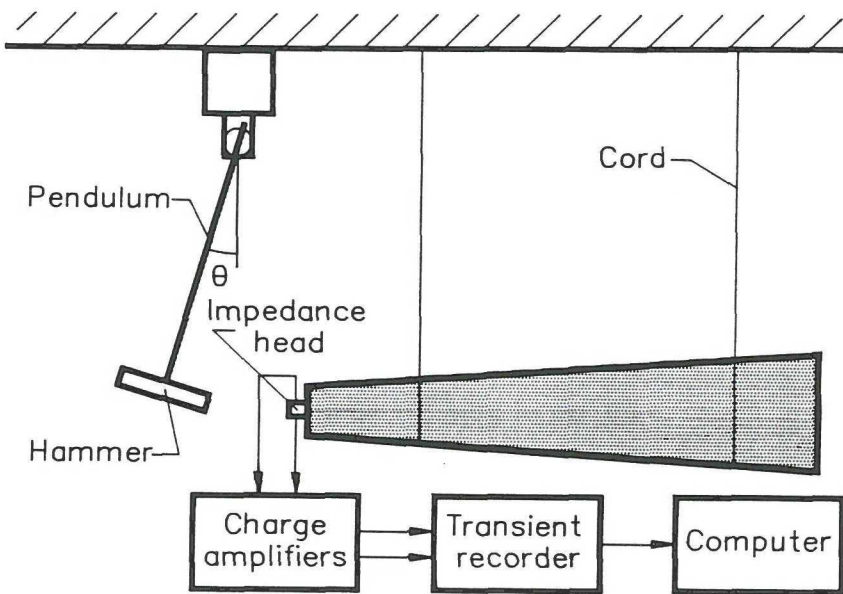


Figure 3. Experimental set-up for impulse response tests.

The signals from the impedance head (Brüel & Kjær 8001), representing the force F_1 and the acceleration dv_1/dt , were amplified by two charge amplifiers (Brüel & Kjær 2635) and recorded by a transient recorder (Data Precision 6100). The acceleration was integrated once by the transient recorder to give the velocity v_1 . Furthermore, the auto-spectrum of the force and the cross-spectrum from force to velocity were computed by the transient recorder. These discrete spectra were transferred to a computer (HP 9100) which computed the discrete Fourier transform of the impulse response G_1 (the mobility) as the ratio of average spectra from ten tests for each of the two hammers. The results for the two hammers were combined by choosing, for each discrete frequency, the result corresponding to the

largest average auto-spectrum of the force. Generally, this means that the results obtained with the heavy hammer dominated at lower frequencies, while those obtained with the light hammer dominated at higher frequencies. The sample period was 28 ms and the number of samples was 4096, which corresponds to a duration of measurement of 115 ms. In order to avoid aliasing errors only the low-frequency halves of the spectra, that is, frequencies up to 8.9 kHz, were used.

3.2. Prediction

The impulse responses G_1 were also predicted for the four cases TCA, TCB, CCA, CCB. In addition, the impulse response G_2 was predicted for a long cylindrical rod (LCR) made of steel. Its length was 6150 mm and its diameter was 10 mm. One-dimensional theory was used, and each cross-section was considered to be homogeneous, that is, the effect of holes and screws were neglected. The long cylindrical rod was considered to be semi-infinite (no reflected wave during the time interval of interest).

The results for the Fourier transforms of the impulse responses were expressed in terms of the wave propagation coefficient

$$\gamma = \alpha + ik = i\omega(E/\rho)^{-1/2} \quad (4)$$

and the characteristic impedance

$$Z = R + iX = A(E\rho)^{1/2} \quad (5)$$

where ω is the angular frequency, $E = E(x, \omega)$ the complex modulus, $\rho = \rho(x)$ the density, and $A = A(x)$ the cross-sectional area. Thus, γ and Z are generally functions of x and ω , where x is an axial coordinate. The damping coefficient α is a non-negative even function of ω , while k is an odd function of ω , positive for $\omega > 0$ [13].

From Equations (4) and (5) it follows that the real and imaginary parts of the characteristic impedance Z are related to those of the wave propagation coefficient γ through

$$R = A\rho\omega k / |\gamma|^2, \quad X = A\rho\omega\alpha / |\gamma|^2. \quad (6)$$

From Equations (4) to (6) and the properties of α and k it also follows that γ and Z are replaced by their complex conjugates when ω is replaced by $-\omega$.

For Nylon-6 the approximate relations, in terms of SI units,

$$\alpha = 8.818 \cdot 10^{-5} \omega^{0.894}, \quad k = 8.937 \cdot 10^{-4} \omega^{0.970} \quad (7)$$

were established for $\omega > 0$ up to 10 kHz on the basis of experimental results [14]. The density was 1150 kgm^{-3} . For aluminium the complex modulus was real, 69 GPa, and the density was 2700 kgm^{-3} . For steel the corresponding data were 206 GPa and 7780 kgm^{-3} , respectively.

For the impact face A of the truncated cone the the Fourier transform of G_1 is

$$\hat{G}_{TCA}(\omega) = \frac{a}{Z_A} \frac{1-b \coth(b-a)}{1-ab-(b-a) \coth(b-a)} \quad (8)$$

where $a = \gamma x_A$, and $b = \gamma x_B$. The quantities x_A and x_B are the distances from the apex to the ends A and B of the truncated cone, respectively.

For the impact face A of the compound cylinder there is the corresponding result

$$\hat{G}_{CCA}(\omega) = \frac{1}{Z_A} \frac{\phi^3 + 3ab\phi^2 + (a^2b^2 + a^2 + b^2)\phi + ab}{a\phi^3 + b(2a^2 + 1)\phi^2 + a(2b^2 + 1)\phi + b} \quad (9)$$

where $a = \coth(\gamma_A L)$, $b = \coth(\gamma_B L)$ and $\phi = Z_B/Z_A$. In these relations A and B refer to the materials at the ends A (Nylon-6) and B (aluminium) of the compound cylinder.

The results for the impact faces B were obtained by replacing A by B and interchanging the roles of a and b in Equations (8) and (9), by changing the sign of the right member of Equation (8), and, finally, by replacing ϕ by ϕ^{-1} in Equation (9).

For the long cylindrical rod the Fourier transform of G_2 is

$$\hat{G}_{LCR}(\omega) = \frac{1}{Z} \cdot \quad (10)$$

Derivations of Equations (8)-(10) are given in the Appendix.

Discrete Fourier transforms of the impulse responses G were obtained, finally, by sampling the corresponding Fourier transforms. Frequencies up to 10 kHz were used, and the number of samples was 2048.

4. IMPACT FORCE AND RESULTS

Four different impact tests were carried out, corresponding to different combinations of impacting bodies. The first impacting body, with impulse response G_1 , was the truncated cone with impact face A or B, or the compound cylinder with impact face A or B. The second impacting body, with impulse response G_2 , was the long cylindrical rod. The impact force histories $F(t)$ were measured with the aid of a pair of strain gauges on the long cylindrical rod. They were also predicted on the basis of the measured as well as the predicted impulse responses G_1 and the predicted impulse response G_2 , using the impulse response method.

The experimental set-up is shown in Figure 4 for the tests involving the truncated cone. This body and the long cylindrical rod were suspended in thin cords, and the impact velocity V was determined from the drop height h . For the tests involving the compound cylinder a different arrangement was used for the impacting bodies: The compound cylinder was accelerated by an air gun, and the long cylindrical rod was supported by low-friction slide bearings. In these tests the impact velocity V was determined with the aid of three light beams and photo cells at the muzzle of the gun.

The pair of strain gauges (HBM LG11) was mounted on the long cylindrical rod 150 mm from the impacted end. The two gauges had diametrically opposite positions and were connected to a bridge amplifier (Measurement Group System 2200) in such a way that contributions from bending were suppressed. The strain signal was recorded by a transient recorder (Data Precision 6100) with a sample period of 5 ms. The strain data were transferred to a computer (HP 9100) and the impact force was determined from the relation $F(t) = -AE\epsilon(t+t_{tr})$, where t_{tr} is the transit time for a wave from the impacted end to the instrumented cross-section.

The impact velocities determined in the tests with the TCA, TCB, CCA, and CCB were 1.16, 0.93, 0.92, and 1.01 ms^{-1} , respectively. The measured and the two predicted impact force histories are shown in Figure 5 for the cases

involving the truncated cone, and in Figure 6 for those involving the compound cylinder.

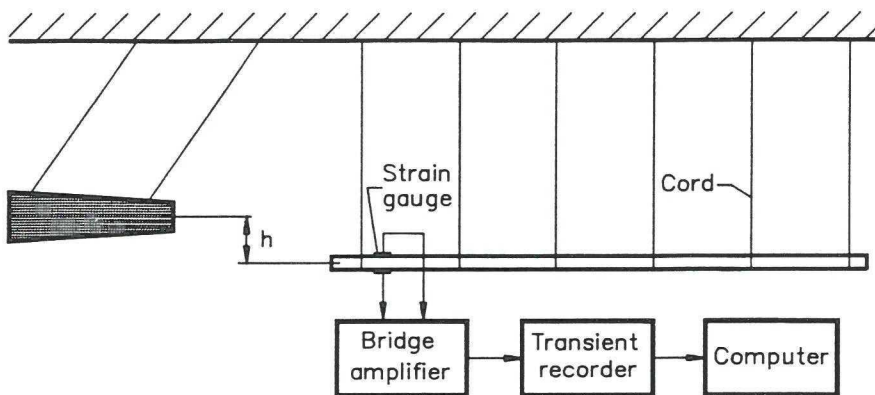


Figure 4. Experimental set-up for impact tests involving the truncated cone.

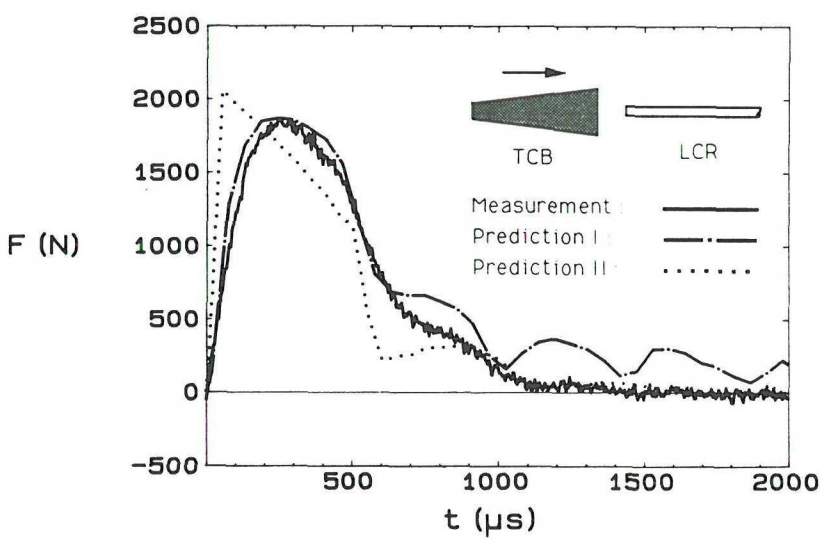
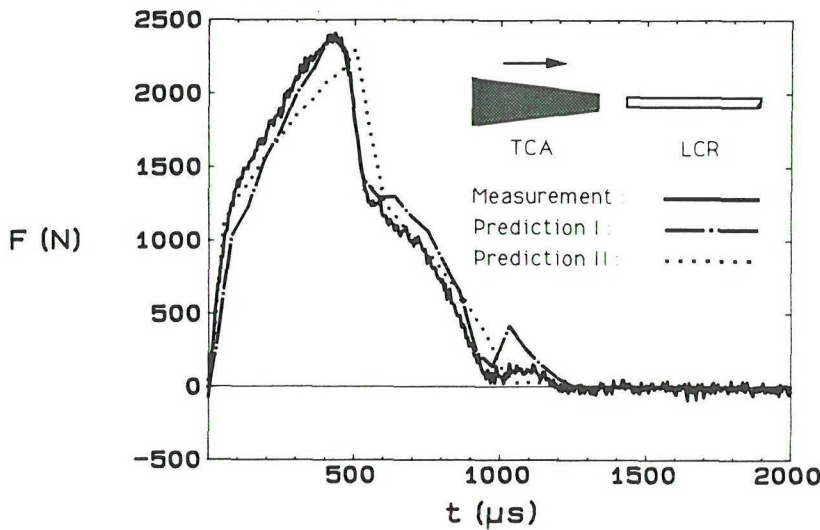


Figure 5. Measured and predicted force histories $F(t)$ for impact between a truncated cone (TC) with impact faces A and B, and a long cylindrical rod (LCR). The predictions are based on impulse responses which are (I) measured for the truncated cone and predicted for the long cylindrical rod and (II) predicted both for the truncated cone and for the long cylindrical rod.

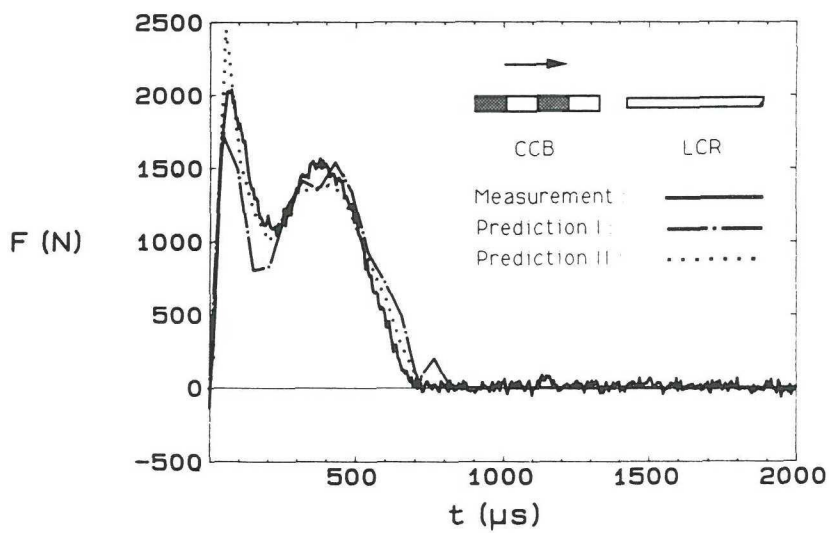
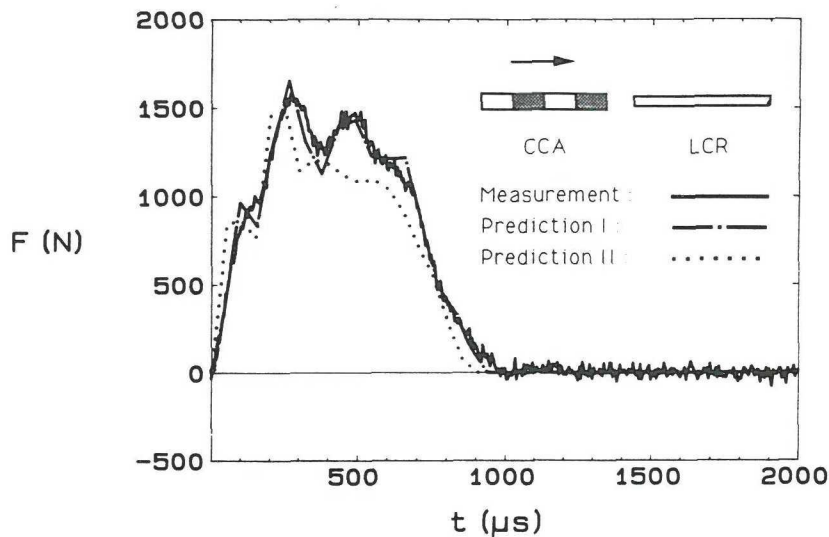


Figure 6. Measured and predicted force histories $F(t)$ for impact between a compound cylinder (CC) with impact faces A and B, and a long cylindrical rod (LCR). The predictions are based on impulse responses which are (I) measured for the compound cylinder and predicted for the long cylindrical rod and (II) predicted both for the compound cylinder and for the long cylindrical rod.

5. DISCUSSION

From the results obtained it is concluded that the impulse response method admits prediction of impact force histories on the basis of measured or predicted impulse responses, or both. The impulse responses, defined by Equations (1), serve to characterize the materials and the geometries of the impacting bodies, and the impact force history is determined from Equations (2) and (3). Thus, if measured impulse responses are used, the method is independent of the complexity of the particular impact problem.

The method has been applied to four cases of impact in two different ways. Firstly, the prediction was based on the measured impulse response G_1 of the first body and on the predicted impulse response G_2 of the second (I). Secondly, it was based on the predicted impulse responses of both of the impacting bodies (II). The third possibility, prediction of impact force based on measured impulse responses of both impacting bodies, was not considered.

The predictions of impulse responses were based on one-dimensional theory, which neglects lateral inertia and requires that initially plane cross-sections remain plane. In all cases of impact considered the conditions for one-dimensional behaviour were amply satisfied by the long cylindrical rod. This was the basis for the measurement of impact force history. This was also the reason why it was not considered necessary to measure the impulse response of the long cylindrical rod. For the truncated cone, especially with impact face B, the conditions for one-dimensional behaviour were less accurately satisfied. In this case, the initially plane cross-section B must have been significantly deformed during impact due to the relatively small diameter and the relatively high stiffness of the long cylindrical rod.

A good general agreement was obtained between both kinds of predictions and measurement of impact force in the four cases of impact studied. Better agreement was obtained for the predictions based on one measured and one predicted impulse response than for those based on two predicted impulse responses. Also, better agreement with measurement was observed in the tests with the compound cylinder than with the truncated cone, and in the test with the impact face A of the truncated cone than in that with the impact face B of the same body. These observations are largely explained by the three-dimensional behaviour of the truncated cone and the compound cylinder; the three-dimensional effects are inherent in the measured but not

in the predicted impulse responses, and they are less important for the compound cylinder than for the truncated cone, and for the impact face A of the truncated cone than for the impact face B of the same body.

When the impulse responses are measured, the exciting forces should ideally act on the anticipated impact faces. In the tests performed, however, they acted only on the approximate central halves of these. This may have given some contribution to the discrepancies observed between predicted and measured impact force histories.

Acknowledgement - The Authors are in debt to the Carl Trygger Foundation, AB Sandvik Rock Tools and Atlas Copco MCT AB for their support. Final parts of the work were done at Laboratoire de Mécanique Physique, Université de Bordeaux I, France.

REFERENCES

1. B. LUNDBERG, Energy transfer in percussive drilling of rock - II Supplement on hammer drilling. *Int. J. Rock Mech. Min. Sci. & Geomech. Abstr.* **10**, 401-419 (1973).
2. S. TANIMURA, A new method for measuring impulsive force at contact parts. *Experimental Mechanics* **24**, 271-276 (1984).
3. K. G. SUNDIN and M. JONSSON, A stiff and compact force transducer based on strain measurement. *Experimental Mechanics* **25**, 48-53 (1985).
4. K. G. SUNDIN and M. JONSSON, A force transducer based on measurement of mean strain in a compact body. *Journal of Strain Analysis* **24**, 31-35 (1989).
5. M. DAIMARUYA, M. NAITOH, H. KOBAYASHI and S. TANIMURA, A sensing-plate method for measuring force and duration of impact in elastic-plastic impact of bodies. *Experimental Mechanics* **29**, 268-273 (1989).
6. B. LUNDBERG and A. HENCHOZ, Analysis of elastic waves from two-point measurement. *Experimental Mechanics* **17**, 213-218 (1977).
7. N. YANAGIHARA, New measuring method of impact force. *Bulletin of the JSME* **21**, 1085-1088 (1978).

8. J. F. DOYLE, Determining the contact force during the transverse impact of plates. *Experimental Mechanics* **27**, 68-72 (1987).
9. H. INOUE, T. SHIBUYA, T. KOIZUMI and R. WATANABE Measurement of impact force history by deconvolution method. *Proceedings of 6th International Congress on Experimental Mechanics*, Portland, Oregon 463-468 (1988).
10. P. E. HOLLANDSWORTH and H. R. BUSHBY, Impact force identification using the general inverse technique. *Int. J. Impact Engng* **8**, 315-322 (1989).
11. C. CHANG and C. T. SUN, Determining transverse impact force on a composite laminate by signal deconvolution. *Experimental Mechanics* **29**, 414-419 (1989).
12. B. LUNDBERG and M. LESSER, On impactor synthesis. *Journal of Sound and Vibration* **58**, 5-14 (1978).
13. S. C. HUNTER, Viscoelastic waves. In *Progress in Solid Mechanics* (I. N. Sneddon and R. Hill, editors). Vol. 1, 3-56, North-Holland, Amsterdam (1960).
14. B. LUNDBERG and R. H. BLANC, Determination of mechanical material properties from the two-point response of an impacted linearly viscoelastic rod specimen. *Journal of Sound and Vibration* **126**, 97-108 (1988).

APPENDIX

Consider a straight, non-uniform and linearly viscoelastic rod with cross-sectional area $A(x)$, complex modulus $E(x,\omega)$ and density $r(x)$, where x is an axial coordinate. The one-dimensional equation of motion and the constitutive equation can be expressed

$$\frac{\partial \hat{N}}{\partial x}(x,\omega) = A(x)r(x)i\omega \hat{v}(x,\omega) \\ A(x)E(x,\omega) \cdot \frac{1}{i\omega} \frac{\partial \hat{v}}{\partial x}(x,\omega) = \hat{N}(x,\omega) \quad (A1)$$

respectively, provided that the Fourier transforms exist. N is the normal force, positive in tension, and v is the particle velocity, positive in the direction of increasing x . These equations can be expressed in terms of the propagation coefficient $\gamma(x,\omega)$ and the characteristic impedance $Z(x,\omega)$, defined by Equations (4) and (5), respectively, as

$$\frac{\partial}{\partial x} \begin{bmatrix} \hat{N} \\ \hat{v} \end{bmatrix} = \begin{bmatrix} 0 & \gamma Z \\ \gamma/Z & 0 \end{bmatrix} \begin{bmatrix} \hat{N} \\ \hat{v} \end{bmatrix}. \quad (\text{A2})$$

Consider first the truncated cone with impact face A. Let the apex be at $x = 0$, and let the end faces A and B be at $x = x_A > 0$ and $x = x_B > x_A$, respectively. Then the characteristic impedance can be expressed

$$Z(x,\omega) = Z_A(\omega)(x/x_A)^2 \quad (\text{A3})$$

for $x_A \leq x \leq x_B$, and the general solution of Equation (A2) is

$$\begin{aligned} \hat{N}(x,\omega) &= (Z_A/\gamma x_A^2)[-C(\gamma x+1)\exp(-\gamma x) + D(\gamma x-1)\exp(\gamma x)] \\ \hat{v}(x,\omega) &= (1/x)[C\exp(-\gamma x) + D\exp(\gamma x)] \end{aligned} \quad (\text{A4})$$

where C and D are arbitrary functions of ω . The Fourier transform of the impulse response is

$$\hat{G}_{TCA}(\omega) = -\hat{v}(x_A,\omega)/\hat{N}(x_A,\omega) \quad (\text{A5})$$

In order to guarantee the existence of the Fourier transform, the end B is not considered free but supported by a linear dashpot with damping coefficient $q > 0$. The desired result is achieved by letting q approach zero. Thus, the boundary condition at B is taken to be

$$\hat{N}(x_B,\omega) = -q\hat{v}(x_B,\omega) \quad (\text{A6})$$

Equations (A4)-(A6) give

$$\hat{G}_{TCA}(\omega) = \frac{a}{Z_A} \frac{1 - b \coth(b-a) - (q/Z_A)a^2/b}{1 - ab - (b-a)\coth(b-a) - (q/Z_A)(a^2/b)[1 + a \coth(b-a)]}. \quad (A7)$$

When $q \rightarrow 0$ there is the result (8).

Consider next the compound cylinder with impact face A at $x=0$ and end face B at $x=4L$. The state at B is related to that at A by

$$\begin{bmatrix} \hat{N}(4L, \omega) \\ \hat{v}(4L, \omega) \end{bmatrix} = P \begin{bmatrix} \hat{N}(0, \omega) \\ \hat{v}(0, \omega) \end{bmatrix} \quad (A8)$$

where P is the transition matrix. In this case, when the properties of the rod are piecewise constant, P can be expressed as the product

$$P = P_B P_A P_B P_A \quad (A9)$$

where

$$P_A = \begin{bmatrix} \cosh(\gamma_A L) & Z_A \sinh(\gamma_A L) \\ (1/Z_A) \sinh(\gamma_A L) & \cosh(\gamma_A L) \end{bmatrix} \quad (A10)$$

is the transition matrix for the sections A, and where, similarly, P_B is the transition matrix for the sections B. The Fourier transform of the impulse response is

$$\hat{G}_{CCA}(\omega) = -\hat{v}(0, \omega)/\hat{N}(0, \omega) \quad (A11)$$

and, similarly as in Equation (A6), the boundary condition at B is taken to be

$$\hat{N}(4L, \omega) = -q\hat{v}(4L, \omega). \quad (A12)$$

Equations (A8)-(A12) give

$$\hat{G}_{CCA}(\omega) = \frac{1}{Z_A} \frac{\phi^3 + 3ab\phi^2 + (a^2b^2 + a^2 + b^2)\phi + ab + (q/Z_A)\phi^2 m(\phi)}{a\phi^3 + b(2a^2 + 1)\phi^2 + a(2b^2 + 1)\phi + b + (q/Z_A)\phi^2 n(\phi)} \quad (A13)$$

where

$$\begin{aligned}m(\phi) &= a\phi^{-3} + b(2a^2+1)\phi^{-2} + a(2b^2+1)\phi^{-1} + b \\n(\phi) &= \phi^{-3} + 3ab\phi^{-2} + (a^2b^2+a^2+b^2)\phi^{-1} + ab.\end{aligned}\tag{A14}$$

When $q \rightarrow 0$ there is the result (9).

Consider finally, for completeness, the long cylindrical rod $x \geq 0$ with impact face at $x = 0$. The general solution of Equation (A2) is

$$\begin{aligned}\hat{N}(x,\omega) &= Z[-C\exp(-\gamma x) + D\exp(\gamma x)] \\ \hat{v}(x,\omega) &= [C\exp(-\gamma x) + D\exp(\gamma x)].\end{aligned}\tag{A15}$$

As there is no wave travelling in the direction of decreasing x , $D = 0$. The Fourier transform of the impulse response is

$$\hat{G}_{LCR}(\omega) = -\hat{v}(0,\omega)/\hat{N}(0,\omega).\tag{A16}$$

Equations (A15) and (A16) give the result (10).